DES-2019-0437
FERMILAB-PUB-19-287-AE

MNRAS 000, 1–17 (2019) Preprint 16 September 2019 Compiled using MNRAS LaTeX style file v3.0

Search for RR Lyrae stars in *DES* ultra-faint systems: Grus I, Kim 2, Phoenix II, and Grus II

C. E. Martínez-Vázquez,[1⋆] A. K. Vivas,[1] M. Gurevich,[1†] A. R. Walker,[1] M. McCarthy,[2] A. B. Pace,[3] K.M. Stringer,[3] B. Santiago,[4,5] R. Hounsell,[6] L. Macri,[3] T. S. Li,[7,8] K. Bechtol,[9,10] A. H. Riley,[3] A. G. Kim,[11] J. D. Simon,[12] A. Drlica-Wagner,[7,8] E. O. Nadler,[13] J. L. Marshall,[3] J. Annis,[7] S. Avila,[14] E. Bertin,[15,16] D. Brooks,[17] E. Buckley-Geer,[7] D. L. Burke,[13,18] A. Carnero Rosell,[19,5] M. Carrasco Kind,[20,21] L. N. da Costa,[5,22] J. De Vicente,[19] S. Desai,[23] H. T. Diehl,[7] P. Doel,[17] S. Everett,[24] J. Frieman,[7,8] J. García-Bellido,[14] E. Gaztanaga,[25,26] D. Gruen,[27,13,18] R. A. Gruendl,[20,21] J. Gschwend,[5,22] G. Gutierrez,[7] D. L. Hollowood,[24] K. Honscheid,[28,29] D. J. James,[30] K. Kuehn,[31,32] N. Kuropatkin,[7] M. A. G. Maia,[5,22] F. Menanteau,[20,21] C. J. Miller,[33,34] R. Miquel,[35,36] F. Paz-Chinchón,[20,21] A. A. Plazas,[37] E. Sanchez,[19] V. Scarpine,[7] S. Serrano,[25,26] I. Sevilla-Noarbe,[19] M. Smith,[38] M. Soares-Santos,[39] F. Sobreira,[40,5] M. E. C. Swanson,[21] G. Tarle,[34] and V. Vikram[41]
(DES Collaboration)

Affiliations are listed at the end of the paper

Accepted 2019 September 12. Received 2019 September 11; in original form 2019 July 4

ABSTRACT

This work presents the first search for RR Lyrae stars (RRLs) in four of the ultra-faint systems imaged by the Dark Energy Survey (DES) using SOAR/Goodman and Blanco/DECam imagers. We have detected two RRLs in the field of Grus I, none in Kim 2, one in Phoenix II, and four in Grus II. With the detection of these stars, we accurately determine the distance moduli for these ultra-faint dwarf satellite galaxies; μ_0=20.51±0.10 mag ($D_\odot$=127±6 kpc) for Grus I and μ_0=20.01±0.10 mag ($D_\odot$=100±5 kpc) for Phoenix II. These measurements are larger than previous estimations by Koposov et al. 2015 and Bechtol et al. 2015, implying larger physical sizes; 5% for Grus I and 33% for Phoenix II. For Grus II, out of the four RRLs detected, one is consistent with being a member of the galactic halo ($D_\odot$=24±1 kpc, μ_0=16.86±0.10 mag), another is at $D_\odot$=55±2 kpc (μ_0=18.71±0.10 mag), which we associate with Grus II, and the two remaining at $D_\odot$=43±2 kpc (μ_0=18.17±0.10 mag). Moreover, the appearance of a subtle red horizontal branch in the color-magnitude diagram of Grus II at the same brightness level of the latter two RRLs, which are at the same distance and in the same region, suggests that a more metal-rich system may be located in front of Grus II. The most plausible scenario is the association of these stars with the Chenab/Orphan Stream. Finally, we performed a comprehensive and updated analysis of the number of RRLs in dwarf galaxies. This allows us to predict that the method of finding new ultra-faint dwarf galaxies by using two or more clumped RRLs will work only for systems brighter than $M_V \sim -6$ mag.

Key words: galaxies: dwarf — galaxies: individual (Grus I, Kim 2, Phoenix II, Grus II) — stars: horizontal-branch — stars: variables: RR Lyrae

⋆ cmartinez@ctio.noao.edu
† Former research inter student

This document was prepared by [DES Collaboration] using the resources of the Fermi National Accelerator Laboratory (Fermilab), a U.S. Department of Energy, Office of Science, HEP User Facility. Fermilab is managed by Fermi Research Alliance, LLC (FRA), acting under Contract No. DE-AC02-07CH11359.

1 INTRODUCTION

The Sloan Digital Sky Survey (SDSS, York et al. 2000) initiated the era of large-area, deep, multi-color imaging sky surveys. One of the results was the discovery of a *new* class of objects, "ultra-faint" dwarf (UFD) galaxies, the first examples being Willman 1 and Ursa Major I (Willman et al. 2005a,b). These UFDs extend the spectrum of properties of "classical" Local Group dwarf galaxies to a lower mass regime (L< $10^5 L_{\odot}$; M_V >–8 mag). Since these first discoveries, more than 50 UFDs have been found in the Milky Way (MW) neighborhood (Simon 2019). UFDs appear to be possibly the oldest and most primitive of galaxies (Bose et al. 2018; Simon 2019). According to the hierarchical galaxy formation model (White & Frenk 1991) large galaxies are built up by the accretion of smaller galaxies; UFDs may be representative of the basic building blocks of the galaxy formation process. If so, then they are excellent probes to test the galaxy formation models and also to study the early Universe.

In the race to find new UFDs, the combination of the wide field of the Dark Energy Camera (DECam, Flaugher et al. 2015) with the large aperture of the CTIO Blanco 4m telescope (*étendue* = collecting area × field of view = 38 $m^2 deg^2$), makes DECam+Blanco the pre-eminent discovery machine in the southern hemisphere. DECam observations, in particular those of the Dark Energy Survey (DES; The Dark Energy Survey Collaboration 2005) and MagLites (Drlica-Wagner et al. 2016) surveys, have contributed to the discovery of more than 20 ultra-faint stellar systems undetectable in the past (e.g., Martin et al. 2015; Bechtol et al. 2015; Koposov et al. 2015; Kim et al. 2015; Kim & Jerjen 2015; Drlica-Wagner et al. 2015; Martin et al. 2016a; Luque et al. 2016, 2017; Torrealba et al. 2018; Koposov et al. 2018; Mau et al. 2019). The fact that many of them are close to the Magellanic Clouds suggests a possible association (e.g., Jethwa et al. 2016; Erkal et al. 2018; Fritz et al. 2018; Jerjen et al. 2018; Kallivayalil et al. 2018). This scenario of *satellites of satellites* is predicted by cosmological simulations at the time of infall (e.g., Sales et al. 2011; Deason et al. 2015; Wheeler et al. 2015; Pardy et al. 2019).

Before the discovery of the UFDs, dwarf galaxies and globular clusters occupied well-defined locations in the M_V vs. half-light radius (r_h) plane. However, for some of the new discoveries, particularly the most compact ones with $M_V \gtrsim$–4 mag (e.g., Contenta et al. 2017), it is not clear whether they are star clusters or UFD galaxies (see Figure 5 in Drlica-Wagner et al. 2015; Conn et al. 2018a,b). Because they are low-mass systems, the scarcity of stars and the large contamination by field stars make the determination of their morphological parameters a challenge. Moreover, since the evolutionary stages of the stars in these systems are not well populated in the Color-Magnitude diagram (CMD), by comparison with the classical clusters and dwarf galaxies, the determination of the distance using isochrone fitting is a very difficult task (see, e.g., Vivas et al. 2016). Identifying members using radial velocities (e.g., Li et al. 2018) and/or obtaining very deep CMDs reaching well below the main sequence turnoff (e.g., Mutlu-Pakdil et al. 2018) can help to improve the distance using the isochrone fitting.

An independent method to improve the distance to these ultra-faint systems is to search for standard candles, such as RR Lyrae (RRL) stars. RRLs are low-mass (~0.6–0.8$M_{\odot}$), core He-burning horizontal branch (HB) stars that pulsate radially with periods ranging from 0.2 to 1.0 day. The most common types of RRLs are the ab-type (RRab) and c-type (RRc). RRab are fundamental pulsators characterized by longer periods (~0.45–1.0 days) and saw-tooth light-curves. RRc are first overtone pulsators and have shorter periods (~0.2–0.45 days), lower amplitudes and almost sinusoidal light variations. RRLs are found in stellar systems which host an old (t>10 Gyr) stellar population (Walker 1989; Catelan & Smith 2015). They are excellent standard candles due to their well-established period-luminosity relation (see e.g., Cáceres & Catelan 2008; Marconi et al. 2015) that have been primarily calibrated with field stars, first using Baade-Wesselink techniques (Fernley et al. 1998) and then trigonometric parallaxes from *HST/Hipparcos* (Benedict et al. 2011) or *Gaia* (Muraveva et al. 2018). Therefore, the detection of at least one RRL in a UFD or star cluster provides an accurate distance independent from other estimates, thus allowing determination of absolute magnitude and physical size. In addition, the presence of RRLs will confirm the existence of old stellar populations in these galaxies and their pulsation properties can also provide clues about the contribution of UFDs to the formation of the Halo of the MW (e.g., Fiorentino et al. 2015, 2017; Vivas et al. 2016).

In this paper, we focus our attention on four ultra-faint systems imaged in the data collected by DES. From the farthest to the closest, they are Grus I, Kim 2, Phoenix II, and Grus II (Kim et al. 2015; Koposov et al. 2015; Bechtol et al. 2015; Drlica-Wagner et al. 2015). We obtain multi-band (*gri*) and multi-epoch photometry in order to search for RRLs in these systems to better constrain their distances and satellite nature.

This paper is structured as follows. In § 2 we present a summary of the observations. In § 3 we explain the details of the data reduction process. In § 4 we describe the detection, classification, and determination of the mean properties of the discovered RRLs in the four ultra-faint satellite systems. In § 5 we discuss each galaxy individually and determine their distances. In § 6 we show the correlation between the number of RRLs and the total magnitude of the host galaxy and how this relation behaves for galaxies fainter than $M_V \gtrsim$ –6 mag. Finally, in § 7 we present the conclusions of this work.

2 OBSERVATIONS

2.1 Targets

Out of the 17 ultra-faint systems published by Koposov et al. (2015), Bechtol et al. (2015) (DES year 1) and Drlica-Wagner et al. (2015) (DES year 2), we decided to choose four of them (Grus I, Kim 2, Phoenix II, and Grus II) based on their visibility during the A-semester, which is when the observing time was granted. We also took into account their extension in the sky so that they can fit within the field of view (FoV) of the Goodman imager (see § 2.2). Table 1 lists the four chosen targets (column 1) with their location (right ascension and declination in columns 2 and 3, and galactic longitude and latitude in columns 4 and 5), total absolute V magnitude (M_V, column 6), reddening (E(B-V), column 7), and some of their structural parameters: half-light radius (rh, column 8), ellipticity (ϵ, column 9), and position angle (PA, column 10).

2.2 Goodman data

The main data for this project were collected in the semester 2016A under NOAO proposal ID 2016A-0196 (PI. Vivas). The instrumentation used was the imaging mode (with the Blue Camera) of the Goodman High Throughput Spectrograph (GHTS, Clemens et al. 2004) at the 4m SOAR telescope, located on Cerro Pachón (Chile) at 2700m above sea level. The *Goodman Imager* is characterized by a circular FoV of 7.′2 diameter sampled at 0.′′15/pix. Given the

Table 1. Morphological properties of the targets.

System	RA (deg)	Dec (deg)	l (deg)	b (deg)	M_V	E(B–V)	r_h (′)	ϵ	PA (°)	Refs.
Grus I	344.176	–50.163	338.680	–58.245	–3.4±0.3	0.008	$1.77^{+0.085}_{-0.39}$	$0.41^{+0.20}_{-0.28}$	4±60	(1)
Kim 2	317.208	–51.163	347.160	–42.074	–1.5±0.5	0.03	0.42±0.10	0.12±0.10	35±5	(2)
Phoenix II	354.993	–54.405	323.692	–59.748	–2.7±0.4	0.01	1.5±0.3	0.4±0.1	156±13	(3)
Grus II	331.02	–46.44	351.14	–51.94	–3.9±0.2	0.01	$6.0^{+0.9}_{-0.5}$	<0.2	–	(4)

Notes.
- The description of the columns can be found in § 2.1.
- RA and Dec are in J2000.
- Reddening values are from Schlegel et al. (1998) and extinction was obtained using Schlafly & Finkbeiner (2011) calibration adjustment to the original Schlegel et al. (1998) reddening map.
- References (Refs.) in the last column are: (1) Koposov et al. (2015), (2) Kim et al. (2015), (3) Mutlu-Pakdil et al. (2018), (4) Drlica-Wagner et al. (2015).

median seeing during our run (~1.″1), we selected 2×2 binning to reduce readout time, and increase the signal-to-noise.

Time-series were collected in the SDSS g, r and i bandpasses for the four ultra-faint systems. The observations were taken under bright time. The exposures times were between 60s and 120s, increasing to 180s and 300s under poor observing conditions. The cadence of our observations was optimized for RRLs. The images were acquired during the four non-consecutive nights (see Table 2), which helped to minimize aliasing in the period determination of RRLs with P~0.5 days. Within a night, individual g, r, and i epochs of each galaxy were taken with a cadence of 30-90 minutes, interspersing with the same procedure for the other targets. This strategy allowed us to obtain ~4-5 epochs per night. The resulting observations are optimal for characterizing the shape of the light curve (i.e., for determining the correct period and the right amplitude) of a RRL. Table 2 lists the details of the SOAR+Goodman observations for each galaxy: observing dates, exposure times, and number of observations acquired.

Three of the targets (Grus I, Kim 2, and Phoenix I) are small enough that a single pointing would cover an area larger than 2×r_h (pointings in columns 2 and 3 in Table 1). However, for Grus II (which has a larger size, r_h=6.0 arcmin) with just one pointing to the center we would cover less than one half area of the system. Therefore, we decided to choose four pointings dithered with a square pattern around the center, minimizing the overlapped areas, in order to strategically cover ~1×r_h of Grus II.

2.3 DECam data

Additional data in the g, r and i bands of the 4 targets were obtained with DECam (Flaugher et al. 2015), a wide FoV camera (3 deg^2, 62 science CCDs, 0.″263/pixel) installed at the prime focus of the Blanco 4-m telescope at Cerro Tololo Inter-American Observatory (CTIO) in Chile, at 2200m above sea level. DECam filters are similar but not identical to SDSS ones (Abbott et al. 2018). We explain later (§ 3.1.3) how we dealt with those differences. The goal of these observations was to supplement the SOAR+Goodman time series. The cadence of the DECam data was not particularly good for RRLs since these observations were taken during small time windows available during engineering runs. All observations were taken under full moon conditions. The median seeing of the DECam data was 1.″2. Table 2 shows the observing dates, exposure times and number of observations obtained for each galaxy with this instrument. The targets were centered in chip N4, one of the central CCDs in DECam. The full FoV of the SOAR+Goodman imager fits within one DECam CCD (which have a FoV of 18′×9′). The Grus II galaxy, which is the largest system observed in this work, benefits from the extended FoV of DECam, allowing us to explore the outermost parts of the galaxy. Table 2 summarizes the DECam observations used in this work.

2.4 DES data

The ~5,000 deg^2 DES footprint was observed with DECam several times in different filters. Therefore, we have also decided to use the multi-band ($grizY$) single epochs from the first three years of the DES (2013-2015). These measurements were internally released by the DES Collaboration in a catalog named DES Y3Q2 (Year 3, Quick Release 2; see Drlica-Wagner et al. 2015; Morganson et al. 2018 for details). Table 2 lists the number of DES observations used in this work.

3 DATA ANALYSIS

The data processing to obtain the final photometric multi-epoch catalog was performed in the same way for the four targets, but using slightly different procedures for Goodman and DECam data. In the next subsections we explain in detail the steps followed for dealing with data from the two different instruments.

3.1 Goodman data

3.1.1 Photometry

Sets of bias exposures were taken during the nights due to the absence of an overscan region in the images. The set of biases that were closest in time was used for processing each object exposure. We found however, that the bias images were stable throughout the night. Dome and sky flats were taken in the afternoon and at sunset, respectively. Images were corrected using conventional IRAF[1] tasks for bias subtraction and flat fielding. For the particular case of i-band images, a starflat was built instead of dome flat, since it gave better results in correcting the fringing. The starflat was built by combining (with the mode) all the i-band exposures taken during the night. In addition, a circular mask was applied to all the images to deal with the shape of the Goodman Imager field, and thus avoiding problems

[1] IRAF (Tody 1986, 1993) is distributed by the National Optical Astronomy Observatories, which are operated by the Association of Universities for Research in Astronomy, Inc., under cooperative agreement with the National Science Foundation.

Table 2. Observing Log.

System	Data source	Dates	Exp. Time (s)	$N_g^{(a)}$	$N_r^{(a)}$	$N_i^{(a)}$
Grus I	Goodman	2016-06-21, 2016-07-15, 2016-07-16, 2016-07-23	60-300	18	18	19
	DECam	2016-07-17, 2016-08-17, 2016-09-15	120	12	11	12
	DES	DES Y3Q2 (within the first three years of DES Survey)	90	3	3	3
Kim 2	Goodman	2016-06-21, 2016-07-15, 2016-07-16, 2016-07-23	160-180	41	39	38
	DECam	2016-07-17, 2016-08-17, 2016-09-15, 2017-04-04, 2017-08-04	120	17	17	17
	DES	Not checked due to the absence of variables	90	–	–	–
Phoenix II	Goodman	2016-06-21, 2016-07-15, 2016-07-16, 2016-07-23	60-180	16	16	16
	DECam	2016-07-17, 2016-08-17, 2016-09-15, 2017-08-04	120	13	13	13
	DES	DES Y3Q2 (within the first three years of DES Survey)	90	6	5	7
Grus II	Goodman	2016-06-21, 2016-07-15, 2016-07-16, 2016-07-23	60-120	22*	22*	21*
	DECam	2016-07-17, 2016-08-17, 2016-09-15, 2017-04-04, 2017-08-04	60	15	15	15
	DES	DES Y3Q2 (within the first three years of DES Survey)	90	4	6	4

$^{(a)}$ N_g, N_r, and N_i refer to the number of epochs obtained for each system.
*These numbers are the mean exposures taken for Grus II per each of the four fields.

of false detections in the corners of the images when running the photometry.

The photometry was performed using DAOPHOT IV and ALLFRAME packages of programs (Stetson 1987, 1994), following the prescriptions described by Monelli et al. (2010) homogeneously for all the targets. An empirical point spread function (PSF) was derived for each image using bright, unsaturated stars with small photometric uncertainty and spread through the entire FoV in order to account for the possible spatial variations. PSF photometry on individual images was obtained with ALLSTAR, and the derived catalogs were registered on a common coordinate system using DAOMATCH/DAOMASTER. A master catalog, used to feed ALLFRAME, was derived retaining all the sources with at least 5 measurements in any band. Additionally, in order to eliminate most of the background galaxies, we used the shape parameter provided by DAOPHOT called *sharpness* (sharp). We selected only those objects from the input list that have $|\text{sharp}| < 0.5$. This way, we removed some background galaxies and also reduced the ALLFRAME processing time.

Finally, to obtain the time series data, we first selected a reference image in each filter, based on the image quality (best seeing, lowest airmass, magnitude limit, taken under photometric conditions). Secondly, the measurements from each image were re-scaled to the reference image using a magnitude shift calculated as the clipped-mean magnitude difference of stars in common with the reference catalog.

3.1.2 Astrometry

The astrometry for our catalogs was obtained using *Astrometry.net*[2] (Lang et al. 2010). The service produces a file (*corr.fits*) for each solution, listing stars in our image and the reference catalog matched (such as USNO-B1 or 2MASS). The *rms* of the residuals is typically less than $\sim0\farcs5$ in RA and less than $\sim0\farcs3$ in Dec.

[2] http://nova.astrometry.net/ Partially supported by the US National Science Foundation, the US National Aeronautics and Space Administration, and the Canadian National Science and Engineering Research Council.

3.1.3 Calibration

All the photometry reported on Goodman data was calibrated to the DECam photometry system. In order to do that, we cross-matched our data with the photometry available from DES DR1[3], which has a photometric precision better than 1% in all bands and a median depth of $g = 24.33, r = 24.08, i = 23.44$ mag at S/N=10 (Abbott et al. 2018). We derived the transformation equations between the instrumental gri-SDSS magnitudes and the gri-DES photometry only for those stars with magnitude uncertainties less than 0.05 mag, obtaining zero-points and color-terms. Color term coefficients were within 1σ among the different targets. The RMS values of the transformations from the instrumental SDSS to the calibrated DES magnitudes were 0.028 mag in g, 0.030 mag in r, and 0.025 mag in i. Finally, we apply the transformation on the rest of the stars.

3.2 DECam data

The procedure to reduce and process the DECam data was different than for SOAR. DECam data was initially reduced by the DECam Community Pipeline (Valdes et al. 2014) for bias, flatfielding, illumination correction, and astrometry. We used a variant of the DoPHOT (Schechter et al. 1993; Saha et al. 2010) package to perform PSF photometry on the images. This custom-made pipeline for DECam data has been used previously in Vivas et al. (2017); Saha et al. (2019). For Kim 2, Phoenix II and Grus I we only processed the CCD N4 since each DECam CCD has a size of $18'\times9'$, which covers completely the area of the SOAR-Goodman FoV. For Grus II, we ran the photometry in the 12 centermost CCDs, covering an area up to $4\times r_h$ of the galaxy. As we did with Goodman data, to build the time series data set we chose reference images, based on seeing conditions, for each galaxy and each filter. All epochs were normalized to the reference image by calculating clipped-mean differences in magnitude using the stars with magnitude uncertainties smaller than 0.05 mag, thus removing spurious measurements. Calibration to the standard DES photometric system was made by measuring the zero-point differences between the reference images and the DES DR1 photometry.

[3] https://des.ncsa.illinois.edu/releases/dr1

3.3 DES data

Regarding the DES data, reduction and photometry for these data are done following the methods and procedures of DES Collaboration. Details about how DES Quick Release catalogs are generated can be found in Drlica-Wagner et al. (2015) and Morganson et al. (2018). Here we extracted the individual epoch photometry for our periodic variable star candidates, as will be explained in the next section.

3.4 Searching for RR Lyrae stars

Starting with our Goodman photometric catalog, we performed the search of periodic variable sources. We visually inspected all the light-curves in our whole catalog, without any cut on a variability index. A periodogram was calculated between 0.2 and 10 days, which is far broader than the range that encompasses all the possible periods of RRLs and Anomalous Cepheids. The periodogram was produced using Fourier analysis of the time series, following Horne & Baliunas (1986) prescriptions. Once periodicity was confirmed, the final period was refined by adding the additional DECam and DES data and visually inspecting the light-curves in the three bands simultaneously.

With 15 DECam epochs per band, Grus II (our most extended target) has enough epochs to attempt to find periodicity in the variable stars outside the Goodman coverage. We indeed found additional RRLs in this galaxy using only the DECam data (see § 5.4).

Pulsation parameters were derived for the confirmed RRLs. Following the procedure described in Bernard et al. (2009), we obtained the intensity-averaged magnitudes and amplitudes by fitting the light-curves with a set of templates based on the set of Layden et al. (1999). In particular, obtaining the mean magnitudes through the integration of the best fitted template avoids biases appearing from light-curves that are not uniformly sampled. The RRLs detected in each system will be discussed in detail in § 4 and § 5. No Anomalous Cepheids were found, indicating that none of these systems contains a significant intermediate-age population, if any.

4 RR LYRAE STARS

We have identified a total of seven RRLs in the fields of three of our four systems: two in Grus I, one in Phoenix II, and four in Grus II. No RRL was found in the field of Kim 2. Individual epoch photometry for all these RRLs is given in Table 3 and light-curves are represented in Fig. 1. The naming of the RRLs satisfies the following pattern. The letter "V" denotes that they are variable stars, followed by a number which represents their right ascension order for each field. Finally, we added a prefix which refers to the name of the system they belong to (see § 5 for more details). The location of these stars (RA and Dec) together with individual pulsation parameters and type are listed in Table 4.

In addition, we cross-checked these detections with two RRL catalogs recently published: Stringer et al. (2019, hereafter S19) and *Gaia* DR2 (Holl et al. 2018; Clementini et al. 2019)[4]. S19 used the DES Y3Q2 catalog to search for RRab stars. Despite the sparse multiband sampling of the DES Y3Q2 data, they identified 5783 RRab to distances within 230 kpc. However, the S19 catalog is incomplete for objects with very few (<20) observation epochs or large distances (see their Figure 14). None of our seven RRLs were recovered in the S19 final RRab catalog due to several different factors: *i)* their large distances (Grus I-V2 and Phoenix II-V1), *ii)* their small number of DES Y3 observations in their light-curves (7 for Grus I-V1 and 15 for Chenab-V4), and *iii)* their short periods[5] (Grus II-V1, Chenab-V2, Halo-V3). Finally, we also look for additional RRL candidates in the S19 catalog in the same area we mapped in this work (4 arcmin for Grus I, Kim 2 and Phoenix II, and 21 arcmin for Grus II) but none were found.

Gaia DR2 flags five of our seven RRLs as variables. However, no association of these stars to the UFDs was made before. *Gaia* only provides pulsation properties for three of them (Phoenix II-V1, Halo-V3, and Chenab-V4). For Phoenix II-V1 and Halo-V3 the periods obtained by *Gaia* are within 0.0001 day to the periods presented in this work, but Chenab-V4 shows a different period in *Gaia* (0.66847 days) that cannot be reproduced with our data. This period may be an alias. In particular, we have downloaded the *Gaia* epoch photometry for this RRL and the light-curve phase-folded matches well to our period (0.620571 days). Grus I-V1, and Grus I-V2 were not detected as variables in *Gaia* DR2, likely because their mean magnitudes are fainter than the *Gaia* limit ($G \lesssim 20.5$ mag). Finally, we use the *Gaia* DR2 catalog to look for RRLs in a more extended region than the search area of our work. The conclusion is that we did not find any RRL that could belong to these systems in a radius of 10 arcmin around Grus I, Phoenix II, and Kim 2, and 30 arcmin around Grus II.

4.1 Period-luminosity-metallicity relation and distance estimates

In order to estimate the distance moduli, (m-M)$_0$ or μ_0, to the RRLs as proxy of the host system, we use the period-luminosity-metallicity relation in the i_{SDSS} band derived by Cáceres & Catelan (2008):

$$\mathrm{M_{i_{SDSS}}} = 0.908 - 1.035 \log \mathrm{P} + 0.220 \log \mathrm{Z}, \quad (1)$$

where P is the period of the RRL and Z is defined by the following equation (Salaris et al. 1993; Catelan et al. 2004) :

$$\log Z = [\mathrm{Fe/H}] + \log(0.638 \times 10^{[\alpha/\mathrm{Fe}]} + 0.362) - 1.765. \quad (2)$$

This period-luminosity-metallicity relation (eq. 1) is based on theoretical models that are consistent with a distance modulus to the Large Magellanic Cloud of (m-M)$_0$=18.47 mag, which is in agreement with previous and recently derived values (see e.g., Walker 2012; Pietrzyński et al. 2019). The standard uncertainty of this relation is 0.045 mag. The choice of the metallicity for each system, and therefore the value of the Z (according with the eq. 2), will be discussed in further detail in the next section.

We decided to use the period-luminosity relation in the i band (eq. 1) to derive the distance modulus because this relation has less scatter than the g and r period-luminosity relations (see Figure 1 in Cáceres & Catelan 2008) and will thus yield more precise distances. Since this relation was obtained for RRLs in SDSS passbands, we first have to transform our i_{DES} mean magnitudes to i_{SDSS} using the following transformation equation obtained by the DES Collaboration[6]:

[4] It is worth noting that we performed the search over the whole Cepheids and RRL *Gaia* catalog thought the Space Science Data Center (SSDC) *Gaia* Portal DR2: `http://gaiaportal.asdc.asi.it`

[5] S19 exclude RRc stars and RRab with periods shorter than 0.44 days.

[6] `http://www.ctio.noao.edu/noao/node/5828#transformations`

Table 3. Photometry of the RR Lyrae stars.

ID	HJD^*_g	g	σ_g	HJD^*_r	r	σ_r	HJD^*_i	i	σ_i
GrusI-V1	57585.8899	21.154	0.023	57585.8884	20.921	0.029	57585.8075	20.826	0.036
GrusI-V1	57585.9195	21.182	0.026	57585.9211	20.935	0.027	57585.9239	20.860	0.034
GrusI-V1	57586.9165	21.005	0.025	57586.9180	20.808	0.024	57586.7296	20.933	0.034
GrusI-V1	57586.9447	20.880	0.025	57585.8490	20.876	0.026	57586.9210	20.768	0.033
GrusI-V1	57585.8467	21.126	0.030	57586.9463	20.723	0.024	57586.8513	20.878	0.035
GrusI-V1	57586.8844	21.067	0.029	57585.8103	20.909	0.027	57561.7373	20.630	0.034
GrusI-V1	57585.8120	21.151	0.039	57586.8828	20.835	0.027	57593.8748	20.562	0.034
GrusI-V1	57586.8166	21.104	0.034	57586.8150	20.963	0.031	57585.8867	20.818	0.039
GrusI-V1	57561.9091	21.049	0.039	57593.8721	20.552	0.029	57586.9491	20.686	0.035
GrusI-V1	57586.7796	21.256	0.038	57585.7050	20.870	0.031	57585.8515	20.835	0.040
...									

*Heliocentric Julian Date of mid-exposure minus 2,400,000 days.
Table 3 is published in its entirety in the machine-readable format. A portion is shown here for guidance regarding its form and content.

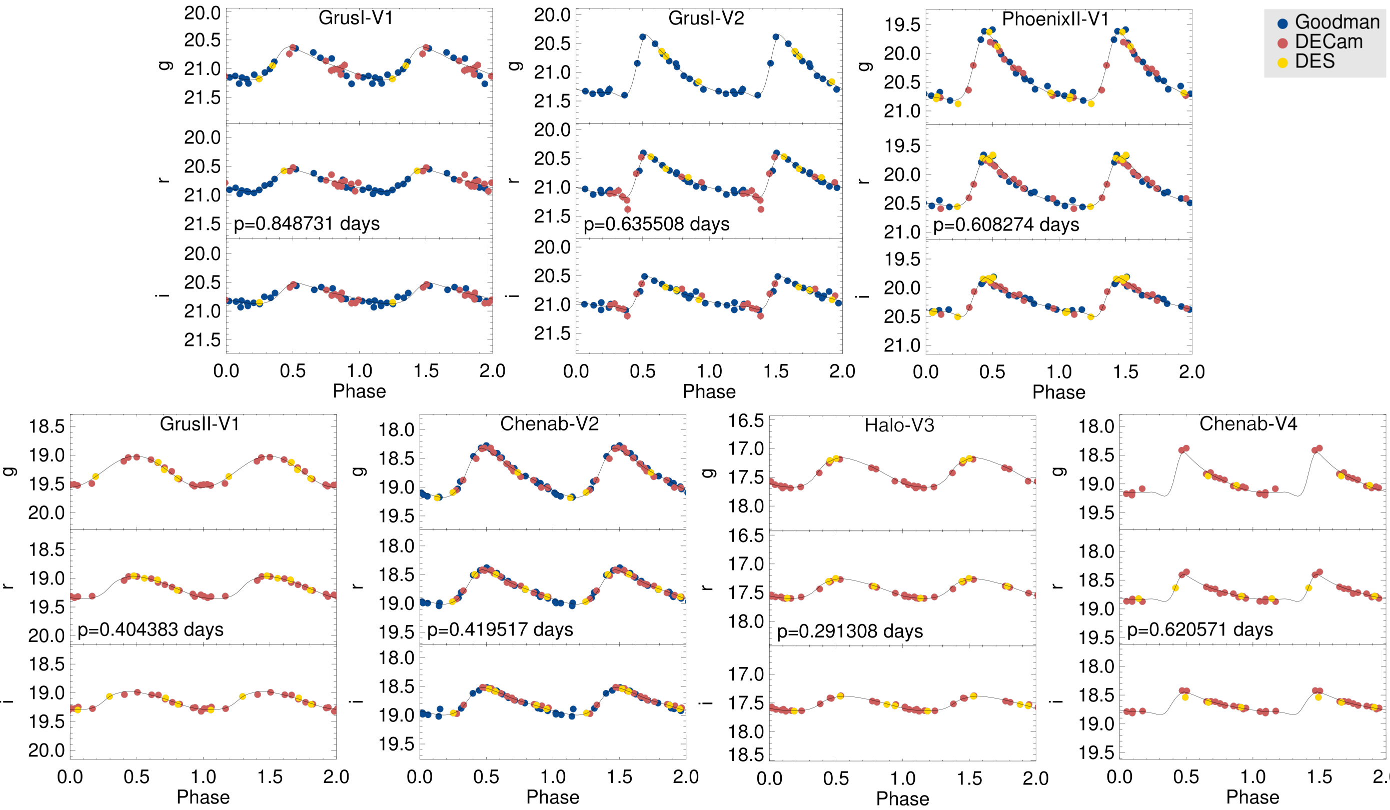

Figure 1. Light-curves of the RRLs detected in this work. All the photometry is presented in DECam photometric system. Solid black lines show the best template fits for each the light-curve. See the text for more details.

$$i = i_{SDSS} + 0.014 - 0.214(i-z)_{SDSS} - 0.096(i-z)^2_{SDSS}, \quad (3)$$

which has a RMS of 0.023 mag. However, this transformation equation has a dependence on a $(i-z)$ color term which we cannot calculate since no z-band exposures were collected in this work. For this reason, following the same approximation made in Torrealba et al. (2018), i.e. based on the small dispersion of the mean $(i-z)$ of the RRLs, we consider that $(i-z)$=+0.013 for RRab and $(i-z)$=–0.006 for RRc stars (calculated from the RRLs in the M5 globular cluster by Vivas et al. 2017) as representative values.

In order to obtain the true distance modulus (μ_0), we corrected the i-band photometry with extinction A_i derived as $R_i \times$ E(B-V), where E(B-V) is from the original Schlegel et al. (1998) reddening map (using for each field the values listed in the 7th column of Table 1), and extinction coefficient R_i from the DES DR1, where a calibration adjustment from Schlafly & Finkbeiner (2011) was used. Last two columns in Table 4 list the distance moduli and heliocentric distances ($D_\odot$) to each RRL detected in this work. The uncertainty in

Table 4. Pulsation parameters of the RRL detected in this work.

ID	RA (deg)	Dec (deg)	Type	Period (days)	N_g	$\langle g \rangle$ (mag)	$\sigma_{\langle g \rangle}$ (mag)	Amp_g (mag)	N_r	$\langle r \rangle$ (mag)	$\sigma_{\langle r \rangle}$ (mag)	Amp_r (mag)	N_i	$\langle i \rangle$ (mag)	$\sigma_{\langle i \rangle}$ (mag)	Amp_i (mag)	μ_0 (mag)	$D_\odot$ (kpc)
Grus I field																		
Grus I-V1	344.1972	-50.1535	RRab	0.8487313	30	20.93	0.05	0.58	31	20.76	0.04	0.40	31	20.71	0.04	0.37	20.50±0.10	126±6
Grus I-V2	344.1989	-50.1868	RRab	0.6355080	23	21.00	0.03	1.09	32	20.87	0.04	0.77	32	20.85	0.04	0.59	20.51±0.10	127±6
Phoenix II field																		
Phoenix II-V1	354.9297	-54.4228	RRab	0.6082742	33	20.34	0.04	1.21	33	20.22	0.03	0.88	35	20.21	0.03	0.69	20.01±0.10	100±5
Grus II field																		
Grus II-V1	330.8729	-46.2809	RRc	0.4043830	21	19.27	0.02	0.55	21	19.16	0.02	0.40	20	19.13	0.02	0.33	18.71±0.10	55±2
Chenab-V2	331.0249	-46.4820	RRab	0.4195172	40	18.77	0.02	0.87	43	18.74	0.02	0.61	40	18.78	0.02	0.49	18.13±0.10	42±2
Halo-V3	331.0436	-46.0740	RRc	0.2913080	19	17.41	0.01	0.52	21	17.43	0.01	0.35	21	17.51	0.01	0.26	16.86±0.10	24±1
Chenab-V4	331.3257	-46.6086	RRab	0.6205710	19	18.94	0.02	0.80	20	18.71	0.01	0.49	20	18.68	0.02	0.40	18.21±0.10	44±2

Notes.
- RA and Dec are in J2000.
- N_λ, $\langle\lambda\rangle$, $\sigma_{\langle\lambda\rangle}$, Amp_λ with $\lambda = \{g, r, i\}$ refer to the number of points per light-curve, the intensity-average magnitude, the uncertainty in the intensity-averaged magnitude (obtained by averaging the photometric uncertainties), and the amplitude of the RRL, respectively.
- Periods for the Grus I-V1, Halo-V3, and Chenab-V4 should be treated cautiously since they were not obtained with an optimal cadence.

Table 5. Final distance moduli determined.

Galaxy	N_{RRL}	$\langle\mu_0\rangle$ (mag)	$\sigma_{\langle\mu_0\rangle}$ (mag)	$D_\odot$ (kpc)
Grus I	2	20.51	0.10	127±6
Phoenix II	1	20.01	0.10	100±5
Grus II	1	18.71	0.10	55±2

the individual distance moduli was obtained by propagation of errors considering: *i)* the photometric uncertainty of the mean magnitude (~0.03 mag), *ii)* the dispersion of the filter transformation equation (i-DES to i-SDSS), *iii)* the dispersion of eq. 1, *iv)* the uncertainty that comes from the reddening value (which is usually considered to be the 10% of its value), and *v)* uncertainties of 0.2 dex in [Fe/H] and [α/Fe].

It is important to note that eq. 1 was calculated from simulations where the RRLs lie on the zero age horizontal branch (ZAHB). Nevertheless, although RRLs spend most of their lifetime close to the ZAHB, they do increase slightly in luminosity, before finally rapidly evolving to the AGB. Therefore, on average, an ensemble of RRLs will be slightly brighter than the ZAHB (see e.g., Sandage 1990; Caputo 1997). In order to quantify this systematic effect, we need to know the location of the ZAHB. This is easy to determine when the HB is well populated, but very hard to identify in systems like those studied in this work, which only have a few stars in the HB. Vivas & Zinn (2006) quantify this effect to be 0.08 mag in V-band from a sample of several globular clusters of different metallicities. Following a similar approach, we calculate this effect but on the i band using DECam data available for the M5 cluster (Vivas et al. 2017). We obtain that the dispersion in the magnitude due to evolution is σ_i^{evol}=0.06 mag. Therefore, by adding this in quadrature to the uncertainty discussed in the previous paragraph, we obtain the total uncertainty in the distance modulus.

Finally, the distance moduli determined for the targets presented in this work are listed in Table 5. We refer the reader to the next section in order to know the details about these obtained values.

5 DISCUSSION SYSTEM BY SYSTEM

5.1 Grus I

Grus I is an ultra-faint system (M_V ~–3.4 mag) located at ~120 kpc (μ_0 ~20.4 mag) which was discovered by Koposov et al. (2015) from DES Year 1 public data. This is the most distant object of the four systems.

From its luminosity and its size (r_h=62 pc), Grus I is likely a dwarf galaxy. However, since this galaxy was found near the gaps between CCDs in the DECam camera, its properties should be treated cautiously. More recently, Jerjen et al. (2018), using very deep Gemini/GMOS-S g, r photometric data, determine that the best isochrone fitting for Grus I is characterized by a mean metallicity of [Fe/H]=–2.5±0.3 dex, age of 14±1 Gyr and a distance modulus of 20.30±0.11 mag ($D_\odot$=115±6 kpc), in agreement with Koposov et al. (2015). However, they could not refine the r_h because of the small field of view. Interestingly, they found that Grus I does not have a well-defined center but instead has the presence of two overdensities of main sequence stars (g_0 >23.7 mag) within its r_h on either side of the center. The authors suggest that this distribution is most likely produced by tidal-disruption forces since these two overdensities are aligned with the direction of the LMC, indicating that Grus I is or was a satellite of the LMC.

Follow-up Magellan/M2FS spectroscopy was performed by Walker et al. (2016). They identified seven stars as probable members of Grus I from a sample of more than 100 stars in the line of sight. Based on these seven stars, Walker et al. (2016) measured a mean metallicity of Grus I of $\langle$[Fe/H]$\rangle$=–1.42 $^{+0.55}_{-0.42}$ dex ($\sigma_{[Fe/H]}$ <0.9 dex) and a mean velocity of $v_{los,\odot}$=–140.5$^{+2.4}_{-1.6}$ km/s, but the velocity dispersion could not be resolved. This metallicity value breaks the luminosity-metallicity relation observed in dwarf galaxies (Simon 2019, see his Section 3.1 and Figure 5) since no other ultra-faint dwarf contains so many metal-rich stars. Further spectroscopic follow-up studies in Grus I will be needed to determine if Grus I is actually that metal-rich.

Fig. 2 shows the ($g - r$, g) CMD obtained from our Goodman data. The CMD reveals several potential RRLs at the level of the

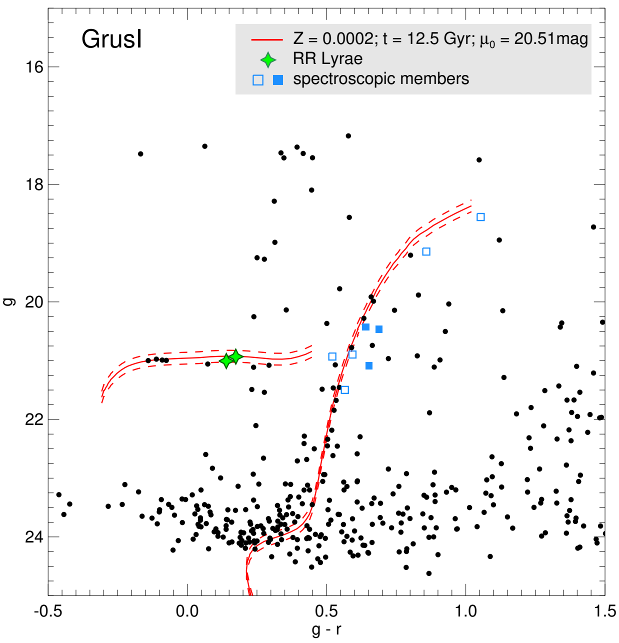

Figure 2. Color-Magnitude diagram for the stars inside a circular field of r≤3.6′∼2×r_h (Goodman FoV) centered on Grus I. The solid red line marks the locus of the isochrone that best fits the features of the CMD to the eye (12.5 Gyr, Z=0.0002) shifted a distance modulus of $(m-M)_0$=20.51 mag, that was obtained from the two RRLs detected (marked as a green stars). Dashed red lines represent the shifted isochrones according to the uncertainty of the distance modulus determination (±0.10). Blue squares represent the updated Walker et al. (2016) spectroscopically-confirmed members (M. Walker, priv. comm.). Filled squares show those that are inside the Goodman FoV and open squares those that lie outside, for which g and r values are taken from DES DR1. Except for this, only Goodman photometry is displayed here.

horizontal branch (HB). In fact, our search results in the detection of two RRLs, one at a distance of 59″ from the center of Grus I (inside the r_h area) and the other at 1′.65, outside the 1×r_h area (see Fig. 3). Three of the spectroscopically-confirmed members by Walker et al. (2016) are within a radius of 3′.6 centered on Grus I, i.e., inside the Goodman FoV (blue filled squares in Fig. 2). Their metallities are [Fe/H] = −2.0, −1.3, and −1.2 dex. We will consider that the most metal-poor star ([Fe/H]=–2.0) may be used as a proxy of the old population, and therefore RRLs, of Grus I. Additionally, based on the α-elements abundance studies performed by Ji et al. (2019), the most reliable measure of such elements in Grus I is [α/Fe]=+0.2 dex. Thus, taking into account the Z-[Fe/H] relationship (eq. 2) we infer Z=0.0002. Therefore, using this value on eq. 1 we derive that the distance of Grus I is μ_0=20.50±0.06 mag (equivalent to $D_\odot$=126±3 kpc), based on the average of the two RRLs. Individual distances are provided in Table 4. It is worth noting that a change of +0.1 dex in [Fe/H] and −0.1 dex in [α/Fe] would be translated in a change of −0.02 and +0.02 mag, respectively, in the estimation of the distance. We overplot a PARSEC isochrone (Bressan et al. 2012) of 12 Gyr and Z=0.0002 in the CMD of Grus I (Fig. 2). The position of this isochrone fits with the two RRLs, as well as with other possible HB members, RGB stars and apparently with MS stars (which is at the limit of our Goodman photometry). Curiously however, the spectroscopically-confirmed members by Walker et al. (2016) within our field, represented by blue filled squares, are redder than of our best isochrone.

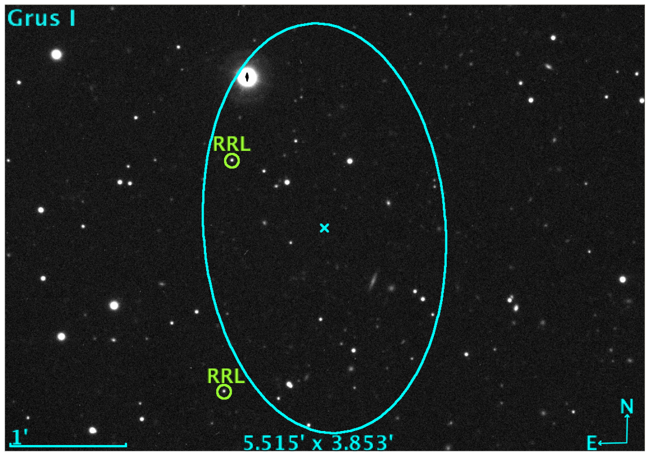

Figure 3. Sky image (from a montage of the 18 r Goodman@SOAR images) of a field of view of 5′.5×3′.9 centered on Grus I. A cyan cross marks the center of the galaxy, and the ellipse displays the half-light radius of this galaxy, accounting for the ellipticity and position angle (values in Table 1). Green circles point out the position of the two RRLs found at a distance of 59″.32 and 1′.65 from the center of Grus I.

The fact that there are two RRLs clumped together in space at this large galactocentric distance is not expected from a smooth distribution of Galactic halo RRLs (e.g., Vivas & Zinn 2006; Zinn et al. 2014). To quantify this, we integrated the number density profile of RRLs derived in Medina et al. (2018), which is appropriate for the outer Halo up to distances of ∼150 kpc. We found that 5×10^{-4} RRLs are expected in an area of 0.011 deg^2, equivalent to the area of the Goodman FoV, in the range of distances between 100 and 150 kpc. Therefore these two RRLs are high confidence members of Grus I. Note that the two RRLs are fainter than the *Gaia* limit ($G \lesssim$20.5 mag) so no proper motions could be obtained for them.

5.2 Kim 2

Kim 2 (M_V ∼–1.5, $D_\odot$ ∼105 kpc, μ_0 ∼20.1 mag; Kim et al. 2015) is another ultra-faint system detected in DES Year 1 (Koposov et al. 2015; Bechtol et al. 2015, also known as Indus I). However, this system had been previously discovered by Kim et al. (2015) using DECam and deep follow-up observations with Gemini/GMOS-S. Based on its compact shape and evidence of dynamical mass segregation, they classified Kim 2 as an outer Halo star cluster, that seems to be more metal-rich ([Fe/H]=–1 dex) and with lower luminosity than other clusters in the outer Halo.

Multiple distance measurements have been obtained for this object: 105, 100, 69 kpc (Kim et al. 2015; Koposov et al. 2015; Bechtol et al. 2015, respectively), all of them based on the isochrone-fitting. We had included this object within our targets with the goal to detect RRLs and obtain an independent distance measurement. However, we report the absence of RRLs in this system based on our Goodman and DECam data.

5.3 Phoenix II

Phoenix II is an ultra-faint satellite (M_V ∼–2.7 mag, $D_\odot$ ∼84 kpc, μ_0 ∼19.6 mag; Mutlu-Pakdil et al. 2018) discovered in DES Year 1 by two independent groups (Bechtol et al. 2015; Koposov et al. 2015). A more recent study by Mutlu-Pakdil et al. (2018) solved

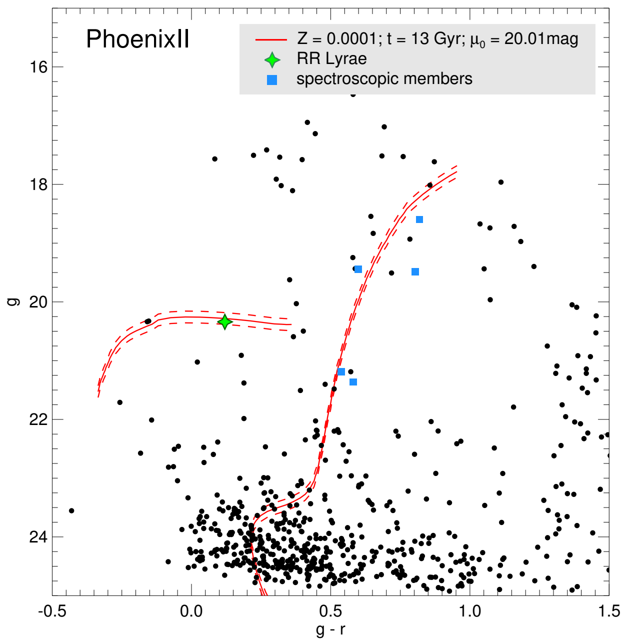

Figure 4. Color-Magnitude diagram for the stars inside the Goodman FoV centered on the Phoenix II (r=3.6 arcmin, ∼2.25×r$_h$). The solid red line marks the locus of the isochrone that best fits the features of the CMD to the eye (13 Gyr, Z=0.0001) shifted a distance modulus of (m-M)$_0$=20.01 mag, that was obtained from the only RRL found (marked as a green star). Dashed red lines represent the shifted isochrones according to the uncertainty of the distance modulus determination (±0.10). Note that only Goodman photometry is displayed here.

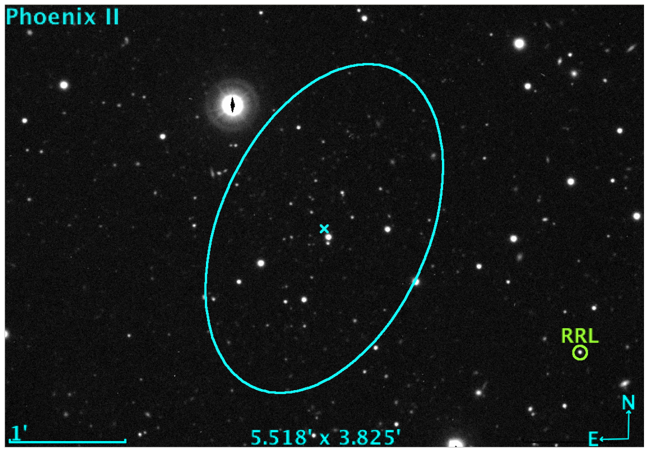

Figure 5. Sky image (from a montage of the 16 r Goodman@SOAR images) of a field of view of 5.′5×3.′8 centered on Phoenix II. A cyan cross marks the center of the galaxy, and the ellipse displays the half-light radius of this galaxy, accounting for the ellipticity and position angle (values in Tab. 1). The green circle indicates the position of the RRL, which is located at a distance of 2.′45 from the center of Phoenix II.

discrepancies in the structural parameters from the previous studies by using deeper photometry from Magellan/MegaCam. The location of this system in the luminosity-half light radius plane makes it a strong candidate to be a dwarf galaxy, supported by spectroscopic measurements. Fritz et al. (2018) found five potential members in this galaxy combining proper motions and photometry from *Gaia* together with intermediate resolution spectra from VLT/FLAMES. They obtained a velocity dispersion of $7.1^{+1.5}_{-1.1}$ km/s, a mean [Fe/H]=–2.75±0.17 dex, and an intrinsic metallicity spread of 0.34 dex.

The location of Phoenix II in the vicinity of the HI Magellanic Stream (see Figure 1 in Jerjen et al. 2018), its kinematics, and photometry, may all indicate that this galaxy is (or was) a satellite of the Magellanic Clouds. This hypothesis is supported by the following studies,

- Fritz et al. (2018) claim the possible prior association with the LMC due to the fact that its orbital pole (∼16°) is close to the orbital pole of the LMC.
- Pace & Li (2019) measure the proper motion of Phoenix II and find that it is consistent with the LMC infall models of Sales et al. (2017) and Kallivayalil et al. (2018).
- The density maps obtained by Jerjen et al. (2018) show that this galaxy has a symmetrical and elongated S-shape structure (around its compact core), where the tidal arms are aligned in the direction of the LMC. They suggest this is evidence of mass loss due to tidal stripping.

Regarding the distance, to date we have only distance measurements from isochrone fittings. Koposov et al. (2015), Mutlu-Pakdil et al. (2018), and Jerjen et al. (2018) set the distance modulus of Phoenix II at ∼19.6 mag, while Bechtol et al. (2015) fix it at 19.9 mag. All of these estimates have uncertainties larger than 0.1 mag.

The ($g-r$, g) CMD of Phoenix II from our Goodman data (Fig. 4) shows few HB stars. Of these one is a RRL located at a distance of 2.′45 from the center of Phoenix II (see Fig. 5). Table 4 lists the pulsation properties for this RRab star and Fig. 1 shows its light curve. Following the procedure described in § 4.1, we determined the distance modulus using this RRL. Adopting [Fe/H]=–2.75 dex (Fritz et al. 2018)[7] and [α/Fe]=+0.2 dex (Jerjen et al. 2018), we obtain Z=0.00004. Thus, the distance modulus of Phoenix II is μ_0=20.01±0.08 mag (D$_\odot$=100±3 kpc). Since extremely metal-poor isochrones (Z<0.0001) are not readily available, we overplot an isochrone of 13 Gyr and Z=0.0001 (Bressan et al. 2012) in the CMD of Phoenix II (Fig. 4). This isochrone fits with the position of the RRL and with the possible two blue HB members. Moreover, out of the five RGB members identified by Fritz et al. (2018, blue squares), four lie close to the isochrone.

The membership of this RRL as a part of the Phoenix II dwarf galaxy is supported from the *Gaia* DR2 proper motion of this star (Lindegren et al. 2018) in comparison to the systemic proper motion of the galaxy obtained by Pace & Li (2019). These particular values are listed in Table 6. Fig. 6 shows the proper motion of the stars that have been identified by Pace & Li (2019) as high probability members (m >0.5 in their definition) of the galaxy based on their proper motions and spatial location (blue dots). The systemic proper motion of Phoenix II is indicated with a red square. The proper motions of the RRL identified in this work (orange symbol) perfectly match those of the other member stars. We also plot the proper motion of an external field described by an area of 1° radius, excluding the

[7] Spectra for the RRL was actually obtained by Fritz et al. (2018, their “phx2_8_24” star). However, the variability of this star was not considered when taking and analyzing the spectra, therefore the values obtained for this star are not reliable. In fact, Fritz et al. (2018) excluded this star when obtaining the mean [Fe/H] of Phoenix II due to its discrepant value compared with the rest of members of Phoenix II.

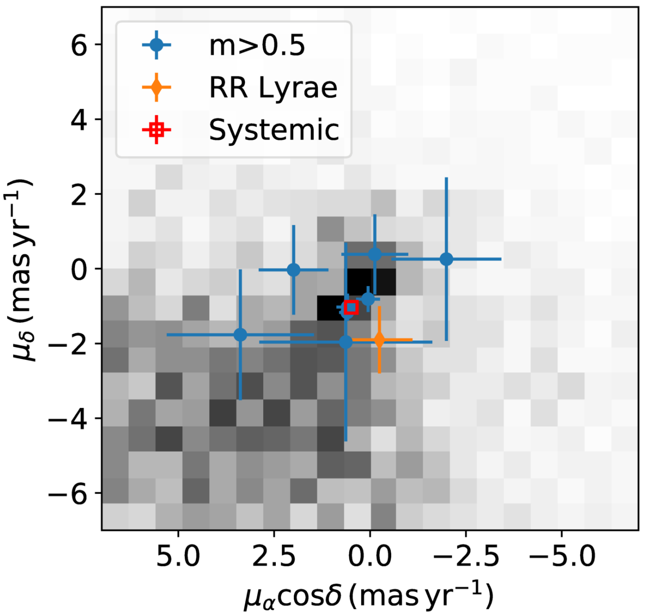

Figure 6. Systemic proper motion of Phoenix II (red square, Pace & Li 2019) and individual proper motions of the members and the RRL from *Gaia* DR2. The grey density map represents the proper motions of the field stars within a circular area defined by a 1° radius centered on Phoenix II (masking the central 5×r_h to remove possible members of Phoenix II). Blue dots represent the high probability members from Pace & Li (2019), while the orange diamond shows the RRL found in this work.

Table 6. *Gaia* DR2 proper motion for Phoenix II and Grus II.

System		RA (deg)	Dec (deg)	$\mu_\alpha \cos(\delta)$ (mas/yr)	μ_δ (mas/yr)
Phoenix II	sys.	354.993	-54.405	0.49±0.10	-1.03±0.12
	V1	354.9295	-54.4228	-0.24±0.86	-1.90±0.90
Grus II	sys.	331.02	-46.44	0.43±0.08	-1.45±0.13
	V1	330.8729	-46.2810	1.21±0.43	-1.28±0.45
	V2	331.0249	-46.4821	0.65±0.34	-1.90±0.40
	V3	331.0437	-46.0741	0.37±0.15	-3.35±0.19
	V4	331.3257	-46.6087	0.48±0.35	-1.47±0.42

central 7.′5 (=5×r_h) in order to be sure that no possible members of Phoenix II would be on it. Although the RRL agrees with the systemic proper motion of the galaxy, the distribution of field stars is also in the same general region in proper motion space. Thus, this alone is not guarantee of membership. However, the statistics for Halo RRLs described for the case of Grus I hold here. We thus conclude it is highly unlikely this is a Halo star and must be then a member of Phoenix II.

5.4 Grus II

Grus II (M_V ∼–3.9 mag) was discovered in the DES Year 2 data (Drlica-Wagner et al. 2015). It is the closest of the systems in our SOAR follow-up sample, at $D_\odot$ ∼53 kpc (μ_0 ∼18.6 mag, Drlica-Wagner et al. 2015). Based on its absolute magnitude and large size (r_h=93 pc), it is classified as a very likely dwarf galaxy (see Figure 4 in Drlica-Wagner et al. 2015). The CMD of Grus II has a large number of HB candidates near g ≃19 mag (see Fig. 7). We needed four Goodman pointings in order to cover 1×r_h (Fig. 8). In addition, we extended our search of variables to an outer region using DECam data (more details in § 3). We found a total of four RRLs in the neighborhood of Grus II; one RRL within ∼0.5×r_h (at 2.52 arcmin from the center) and three more in the outer regions (at 11.32, 16.17, and 21.98 arcmin from the center). The former was found independently in both the Goodman and DECam data, while the other three were identified only in the DECam data since they lie outside of the Goodman coverage. The light-curves of these stars are shown in Fig. 1 and their pulsation parameters and mean properties are listed in Table 4. Fig. 7 shows the position of these stars in the CMD of the central region of Grus II (Goodman photometry).

However, these four RRLs need further discussion regarding their membership in the Grus II system. First, the CMD shows that the RRLs do not all have a similar brightness. In particular, V3 is ∼1.5 mag brighter than the others, hinting that this may be either an Anomalous Cepheid in Grus II or a field RRL. Proper motions provide more insight on these possibilities.

Fig. 9 shows the systemic proper motion of Grus II obtained by Pace & Li (2019) and the individual proper motions of high probability members (m >0.5) of Grus II and the four RRLs. From this plot it is evident that V3 has a proper motion that differs from the systemic proper motion of Grus II by more than 3σ (see also Table 6). Moreover, the star is located beyond 3×r_h of Grus II (see Fig. 8), farther away from the center of Grus II than the other 3 RRLs. Therefore, because of its proper motion, brightness, and location in the sky, V3 is very likely to be a Halo RRL. In fact, if we integrate the number density profile of RRLs derived in Medina et al. (2018), we find that 0.6 RRLs are expected in the range of distances 15-40 kpc in an area of the sky of 0.7 deg^2 centered in Grus II (the area shown in Figure 8). Thus, finding one Halo star at 22 kpc (Table 4) in this field is consistent with expectations from the smooth Halo population.

On the other hand, the RRLs V1, V2, V4 are possible members of Grus II since their proper motions are comparable with the proper motion of its high probability members (see Fig. 9). They also lie within 3×r_h (see Fig. 8). In particular, the RRLs V4 and V2 have proper motions that are very close (within 1σ) to the systemic proper motion, while V1's proper motion is about 2σ away from the systemic proper motion of Grus II. Nevertheless, the proper motions of the field stars belonging to a circular area with a 1° radius centered on Grus II (masking the inner 5×r_h=30′ to avoid any probable member stars from Grus II) do not clearly distinguish the RRLs as members of Grus II or the field.

Interestingly, V2 and V4 have similar brightness, while V1 is $\gtrsim$0.5 mag fainter (see Fig. 7). It is worth noticing that the light curve of the RRL V4 (see Fig. 1) has a poor coverage in its brightest part (i.e., we miss the rising branch of the light curve), therefore it is possible that the magnitude of this star is overestimated by $\lesssim$0.1 mag (due to an underestimation of its amplitude). Thus, we suspect the mean magnitude of V4 may be even closer to that of V2. However, this is not the case for the fainter star V1, which has good phase coverage. Thus, it is very unlikely that the magnitude of this star is underestimated. Note that V1 matches well with the potential blue HB members identified in Drlica-Wagner et al. (2015).

The wide range in magnitude displayed by the three RRLs in Grus II is puzzling. Some possible explanations are:

(i) *Halo stars?* The possibility that any of these 3 stars is a Halo star is quite low. In such a small area, we expect only 0.09 RRLs in the range of 40-60 kpc.

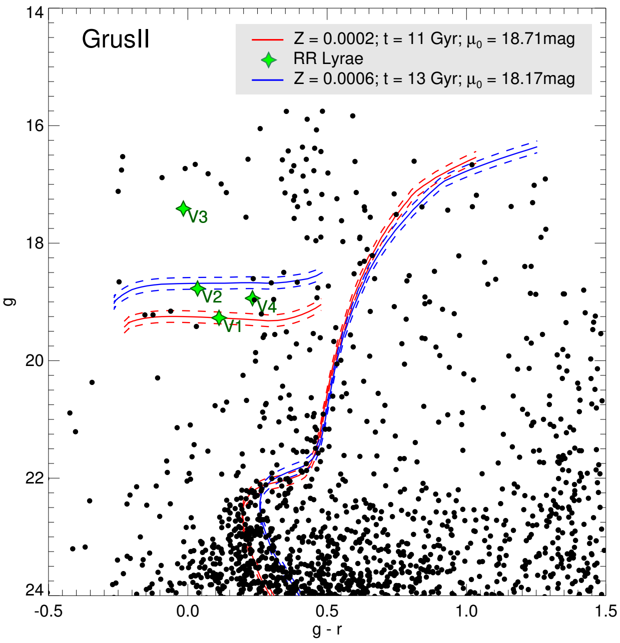

Figure 7. Color-Magnitude diagram of the stars inside r $\lesssim$6 arcmin ∼1×r$_h$ centered on Grus II. RRLs are represented by green symbols. The solid red line marks the locus of the isochrone that best fits the features of the CMD to the eye (11 Gyr, Z=0.0002) shifted a distance modulus of (m-M)$_0$=18.71 mag, that was obtained from the faintest RRL (Grus II-V1). The solid blue line marks the locus of the isochrone that best fits the features of the CMD to the eye (13 Gyr, Z=0.0006) shifted a distance modulus of (m-M)$_0$=18.17 mag, that was obtained from Chenab II-V2 and Chenab II-V4. Dashed red and blue lines represent the shifted isochrones according to the uncertainty of the distance moduli (±0.10). Note that only Goodman photometry is displayed here.

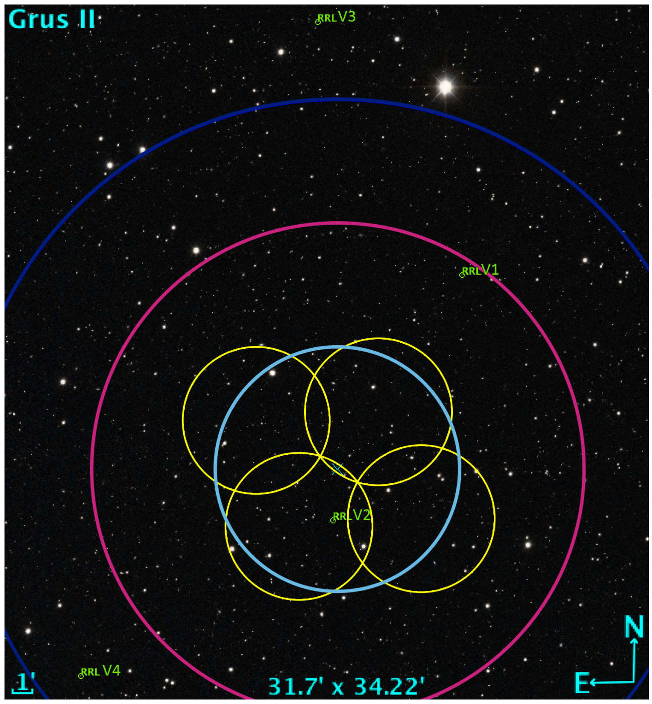

Figure 8. Sky image (from an r-band DES DR1 tile) of a field of view of 31.′7×34.′22 that contains a region >2×r$_h$ of Grus II. A cyan cross marks the center of the galaxy. A cyan circle displays the half-light radius of Grus II while yellow circles show the footprint of the four Goodman's pointings. Magenta and blue ellipses represent 2×r$_h$ and 3×r$_h$, respectively. Green circles point out the four RRLs found in the vicinity of Grus II (at a distance –from V1 to V4– of 11.′32, 2.′52, 21.′98, 16.′17 from the center of Grus II).

(ii) *RRLs evolved from the HB?* In general, dwarf galaxies with hundreds of RRLs show just a few evolved RRLs (see for example Coppola et al. 2015; Martínez-Vázquez et al. 2016). Although it is possible that V2 and V4 are evolved RRLs (hence, brighter), having a system with 2/3 of its RRLs evolved seems unlikely.

(iii) *Anomalous Cepheids?* The period and light curve characteristics of RRLs and Anomalous Cepheids overlap and it is not always easy to distinguish between them. In stellar systems, Anomalous Cepheids are typically $\gtrsim$1 mag brighter than RRLs (see e.g., Martínez-Vázquez et al. 2016). However, V2 and V4 are only ∼0.5 mag brighter than the faintest RRL (V1). Thus, this scenario seems unlikely too.

(iv) *Depth effects within the galaxy?* Assuming Z=0.0002, the distance modulus of the brighter RRLs is ∼18.3 and the faintest, ∼18.7 mag. This corresponds to a difference in distance of ∼9 kpc. Considering that r$_h$ in this system is 80-90 pc, 9 kpc is too much a distance to be a consequence of depth effects within the galaxy.

(v) *Two systems?* On a closer look, the CMD of Grus II (Fig. 7) seems to show two HB sequences. The brighter one, containing V2 and V4, is redder, while the faintest, which contains V1, has more stars in the blue part. Fig. 7 shows two isochrones, one of 13 Gyr and Z=0.0006, and the other 11 Gyr and Z=0.0002, shifted to the distances given by the RRLs in each sequence. The justification for a more metal-rich isochrone for the brighter sequence comes from the fact that the HB appears to have a significant population of red stars. This type of morphology of the HB is usually interpreted as coming from a high metallicity or younger age population. It is known, however, that other parameters are involved in the HB morphology (see Catelan 2009). Moreover, V2 has a period <0.48 d and an amplitude of ∼0.87 mag in g-band, hence it is considered a high-amplitude short-period (HASP) RRL (Fiorentino et al. 2015). HASP stars only appear in systems with old population and metallicities [Fe/H] >–1.5 dex. Radial velocities are needed to further study this stellar system and unravel whether Grus II is actually two separate systems.

(vi) *RRLs from the Chenab/Orphan stream?* The Orphan Stream is a thin, long structure first discovered in the northern hemisphere (Grillmair 2006; Belokurov et al. 2007) but later traced to the Southern hemisphere. The Stream can be traced with RRLs (Sesar et al. 2013; Fardal et al. 2019; Koposov et al. 2019). Although there have been suggestions that the progenitor of this Stream was the Ursa Major II dSph (Fellhauer et al. 2007), recent investigations seem to link it to Grus II (Koposov et al. 2019). Using *Gaia* RRLs, Koposov et al. (2019) traced the Orphan Stream over ∼210 degrees. They discovered that the recently discovered Chenab Stream in the DES footprint (Shipp et al. 2018) is actually part of the Southern extension of the Stream. The Chenab Stream and Grus II satellite are coincident in projection and proper motion coordinates (Koposov et al. 2019, suggest there is a connection between the two substructures), however, Grus II is ∼10 kpc more distant than the Stream. The two brighter RRLs (V2 and V4) are at the correct distance to be Stream members and, in fact, they were pointed as likely Orphan Stream RRLs by Koposov et al. (2019). The Orphan Stream is thought to be from a more massive dwarf galaxy (Sales

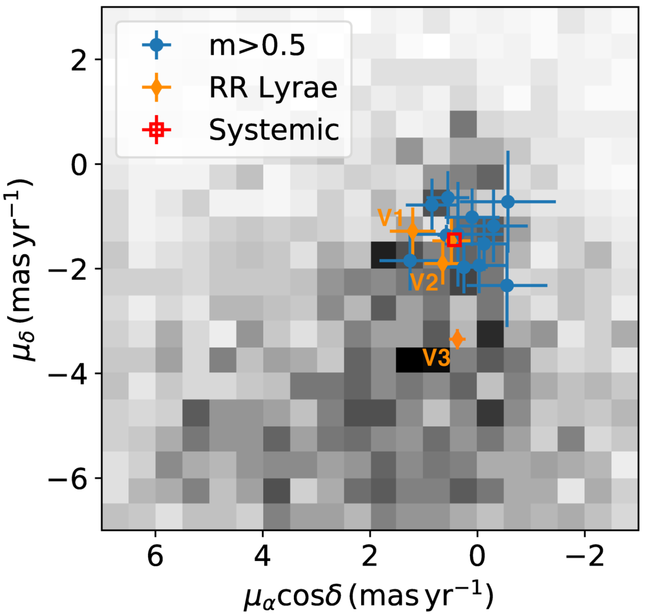

Figure 9. Systemic proper motion of Grus II (red square, Pace & Li 2019) and individual proper motions of the members and RRLs from *Gaia* DR2. The grey density map represents the proper motions of the field stars within a circular area defined by a 1°radius centered on Grus II (masking the central 5×r_h to remove possible members of Grus II). Blue dots represent the high probability members while orange diamonds show the RRLs found within 4×r_h from the center of Grus II.

et al. 2008) similar in size/stellar-mass to some known dwarfs with an RRL population. This may explain the HASP RRL (V2) in the Grus II field of view. Moreover, the proper motions of the two RRLs match both Grus II and the Orphan Stream. Since they are closer to us than Grus II it is likely that they are members of the Stream. Radial velocities of the Chenab/Orphan Stream, Grus II, and the RRLs are required to confirm their membership.

In summary, taking account of the considerations detailed above, out of the four RRLs detected in the field of Grus II, V3 is a very likely Halo RRL, V1 is consistent with being a Grus II member, and from the latter discussion, V2 and V4 seem to be members of the Chenab/Orphan Stream. In order to obtain their distance moduli, we have assumed a [α/Fe]=+0.2 dex and a metallicity of [Fe/H]=–2.0 dex for V1 (Grus II), [Fe/H]=–1.5 dex for V2 and V4 (based on the appereance of the HASP RRL), and [Fe/H]=–1.65 dex for V3 (mean metallicity of the Galactic Halo, Suntzeff et al. 1991). The distance moduli and heliocentric distances to each of these RRLs are shown in the last two columns of Table 4.

6 NUMBER OF RRLS IN DWARF GALAXIES

In recent years there has been increasing interest in using RRLs as a way to uncover unknown stellar systems in the distant Galactic halo (Sesar et al. 2014; Baker & Willman 2015; Sanderson et al. 2017). Since old populations are ubiquitous in all dwarf satellites, they should contain RRLs. And indeed that seems to be the case since RRLs have been found in almost all the systems in which suitable variability studies exist. In the last few years several new low-luminosity systems have been searched for RRLs, including the ones presented in this work. It seems appropriate to revisit the production of RRLs in low-luminosity galaxies.

Fig. 10 shows the number of RRLs (N_{RRL}) as a function of the absolute magnitude of the host dwarf galaxy. It includes satellite galaxies of both the MW (dots) and M31 (squares), Local Group isolated dwarfs (upward triangles), and two Sculptor group dwarf galaxies (downward triangles). Data for this plot are available in Table A in the Appendix. Error bars display the uncertainties of M_V (see column 4 in Table A) and the Poisson errors of N_{RRL}. Not all galaxies have a complete census of their RRL population. We have marked with solid blue symbols those whose studies cover an area enclosing at least 2×r_h, which should contain the majority of the population. There is a clear trend in the number of RRLs as a function of M_V for brighter galaxies, indicated by the fit represented with the red line:

$$\log N_{RRL} = -0.29(\pm0.02)\, M_V - 0.80(\pm0.14) \quad \text{(Pearson correlation, r = -0.96)} \qquad (4)$$

We performed this fit using the linear least squares technique to the log N_{RRL} versus M_V for those dwarf galaxies for which the RRL search was carried out further than 2×r_h, and for which we expect a ~100% of completeness in the number of RRLs (filled symbols). Understandably, galaxies in which the search for variables has not been complete lie below that line. The trend however breaks down for UFD galaxies. Most lie below the line, and no trend is apparent in this low luminosity regime. Out of the 21 UFDs (M_V >–6) that have been searched for RRLs only 10 (48%) have 2 or more RRLs. Fainter than M_V=–3.0, all UFDs have N_{RRL} ≤1. Willman 1 and Carina III (M_V ~–2.5) are the only systems, until now, for which no RRLs have been detected (Siegel et al. 2008; Torrealba et al. 2018). The low number of RRLs in UFDs is not unexpected. The low mass of these galaxies prevents strong events of star formation, which translates to a low rate of RRLs and other stars as well, as is evident from the low number of evolved stars in the upper part of the CMDs of these galaxies. The lack of a trend in N_{RR}-M_V for some of the UFDs, and the fact that there may be galaxies with no RRLs at all, is explained by the Poisson errors in the number of RRLs in the UFDs.

The above warns that although using a single, distant RRL as a tracer of an undercover stellar system is still valid (only 2 out of 21 UFD galaxies have no RRLs), the method suggested by Baker & Willman (2015) of identifying groups of 2 or more RRLs to uncover hidden galaxies may be efficient only for systems with $M_V \lesssim$–6.

7 CONCLUSIONS

Thanks to the high-cadence time series photometry in the g, r, and i bands obtained with Goodman at SOAR, and also with the support of low-cadence g, r, and i data obtained with DECam at CTIO, we have detected seven RRLs in this work: two members of Grus I, none of Kim 2, one of Phoenix II, and one of Grus II, plus two likely members of the Chenab/Orphan Stream and one Halo RRL (which are located along the same line of sight as Grus II).

The detection of these RRLs allows us to set accurate distances to these systems. We obtained a distance modulus of 20.51±0.10 mag ($D_\odot$=127±6 kpc) for Grus I and of 20.01±0.10 mag ($D_\odot$=100±5 kpc) for Phoenix II. These distances are larger than the previous estimations, which imply that their physical sizes are also larger; 5% for Grus I: r_h=65 pc, and 33% for Phoenix II: r_h=44 pc.

A particularly complex case is Grus II. Four RRLs were found

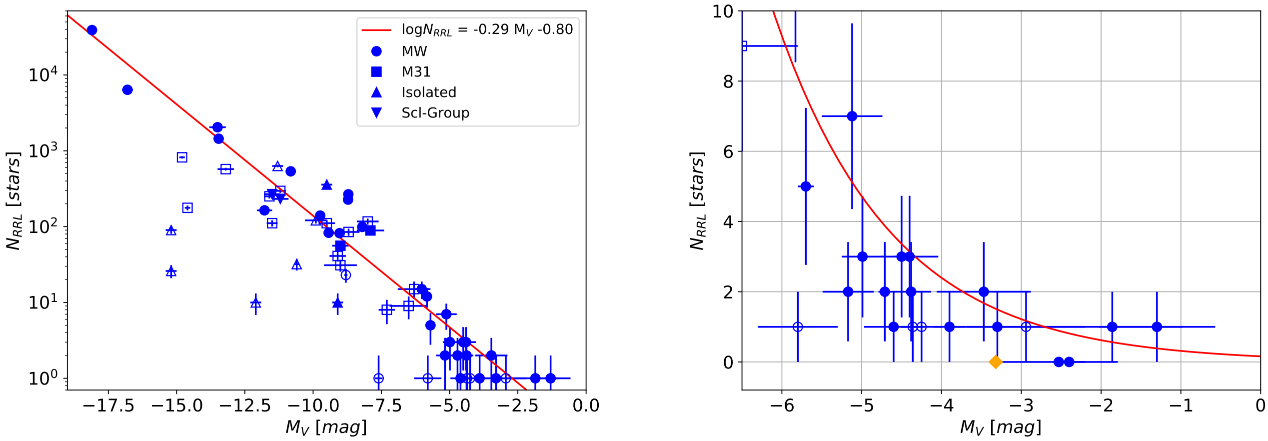

Figure 10. Current literature number of RRLs versus the absolute magnitude of the galaxy, M_V. Blue filled symbols represent those dwarf galaxies for which the RRL search was carried out further than $2\times r_h$, and for which we expect a ~100% of completeness in the number of RRLs. Blue open symbols correspond to those galaxies where either the search for RRLs did not reach $2\times r_h$ or the study was not complete in terms of RRL detection. Different symbols represent different systems: dots represent MW dwarf satellites; squares, M31 dwarf satellites; upward triangles, isolated Local Group dwarf galaxies; downward triangles, Sculptor Group dwarf galaxies. Error bars are also plotted for each galaxy. The red line shows the linear fit between log N_{RRL} versus M_V for the filled symbols. The right panel is a zoom-in of the faint part ($M_V \gtrsim -6$ mag) of the left panel (here without the logarithmic scale in the ordinate axis). N_{RRL}=0 corresponds to Carina III, Willman 1, and Kim 2. Despite not being a dwarf galaxy, Kim 2 (orange diamond) is included in this plot because it is a target in this work. The red line represents the same fit as in the left panel. Note that this panel is not in semi-logarithmic scale.

in the neighborhoods of the system. One of them is consistent with being a Halo member (at a heliocentric distance of 24±1 kpc, μ_0=16.86±0.10 mag). Two of the other three RRLs are located ~0.5 mag above the previously determined HB for Grus II, in which the other RRL is located. This suggests the presence of two systems in the line of sight of Grus II, one at 55±2 kpc, μ_0=18.71±0.10 mag, and the other one at 43±2 kpc, μ_0=18.17±0.10 mag. We associate the former with Grus II, while the latter is likely a different system in front of the UFD. The detection of a subtle red horizontal branch at the level of these two brighter RRLs supports this scenario.

No HASP RRLs have been detected so far in an UFD galaxy (see Figure 10 in Vivas et al. 2016, to see periods and amplitudes of UFD RRLs). This is still the case after our study of Phoenix II, Grus I, and Grus II. However, one of the RRL in the system in front of Grus II can be classified as HASP RRL since it has a short period (P<0.48 d) and large amplitude. HASP RRLs appear in systems more metal-rich than [Fe/H]>−1.5 (Fiorentino et al. 2015). Particularly, they have only been found in systems that were dense or massive enough to enrich up to this metallicity before 10 Gyr ago (Fiorentino et al. 2017). Therefore, according to these facts, the system we find in front of Grus II, which is ~7 kpc closer, may be a remnant of a massive galaxy presumably disrupted who suffered a metal enrichment in its early epoch. Since part of the Chenab/Orphan Stream is crossing the field of view of Grus II, the most probable scenario is the one in which these two RRLs belong to this Stream. Future radial velocities studies in this galaxy will help to decipher the nature of Grus II and its metal-rich neighbor system.

APPENDIX A: NUMBER OF RR LYRAE STARS IN DWARF GALAXIES

Table A is an updated compilation of studies of RRLs in dwarf galaxies. It is sorted by the galaxies' total luminosity, shown in column 4. The total number of RRLs for each galaxy (according with the literature to date) is listed in column 5. Column 6 is a flag that indicates if the catalog of the RRLs (or the search for them) for a particular galaxy goes beyond $2\times r_h$ ($F_{2\times r_h}$=1) or not ($F_{2\times r_h}$=0).

ACKNOWLEDGEMENTS

We thank the anonymous referee for the useful comments that helped to improve the manuscript. CEMV thanks M. Monelli for photometry advices and helpful conversations. RH is partially supported by NASA grant NNH15ZDA001N-WFIRST.

Based on observations obtained at the Southern Astrophysical Research (SOAR) telescope (NOAO Prop. ID 2016A-0196; PI: Vivas), which is a joint project of the Ministério da Ciência, Tecnologia, Inovações e Comunicações (MCTIC) do Brasil, the U.S. National Optical Astronomy Observatory (NOAO), the University of North Carolina at Chapel Hill (UNC), and Michigan State University (MSU).

Based on observations at Cerro Tololo Inter-American Observatory (CTIO), National Optical Astronomy Observatory (NOAO Prop. ID: 2016A-0196, PI: Vivas; NOAO Prop. ID 2012B-0001; PI: J. Frieman), which is operated by the Association of Universities for Research in Astronomy (AURA) under a cooperative agreement with the National Science Foundation (NSF).

Funding for the DES Projects has been provided by the U.S. Department of Energy, the U.S. National Science Foundation, the Ministry of Science and Education of Spain, the Science and Technology Facilities Council of the United Kingdom, the Higher Education Funding Council for England, the National Center for Supercomputing Applications at the University of Illinois at Urbana-Champaign, the Kavli Institute of Cosmological Physics at the University of Chicago, the Center for Cosmology and Astro-Particle Physics at the Ohio State University, the Mitchell Institute for Fundamental Physics and Astronomy at Texas A&M University, Financiadora

Table A1. Number of RR Lyrae stars in dwarf galaxies

Galaxy	RA	Dec	M_V	N_{RRL}	$F_{2\times r_h}$[a]	References[b]
LMC	80.8938	-69.7561	-18.1±0.1	39082	1	MC12; Soszyński et al. (2016)
SMC	13.1867	-72.8286	-16.8±0.2	6369	1	MC12; Soszyński et al. (2016)
NGC 6822	296.2358	-14.7892	-15.2±0.2	26	0	MC12; Baldacci et al. (2005)
IC 1613	16.1992	2.1178	-15.2±0.2	90	0	MC12; Bernard et al. (2010)
NGC 185	9.7417	48.3375	-14.8±0.1	820	0	MC12; Monelli et al. (2017)
NGC 147	8.3004	48.5089	-14.6±0.1	177	0	MC12; Monelli et al. (2017)
Sagittarius dSph	283.8313	-30.5453	-13.5±0.3	2045	1	MC12; Soszyński et al. (2014)
Fornax	39.9971	-34.4492	-13.5±0.1	1443	1	M18; Fiorentino et al. (2017)
Andromeda VII	351.6321	50.6758	-13.2±0.3	573	0	MC12; Monelli et al. (2017)
Leo A	149.8604	30.7464	-12.1±0.2	10	0	MC12; Bernard et al. (2013)
Leo I	152.1171	12.3064	-11.8±0.3	164	1	M18; Stetson et al. (2014)
Andromeda II	19.1117	33.4353	-11.6±0.2	251	0	M16; Martínez-Vázquez et al. (2017)
ESO410-G005	3.8817	-32.1800	-11.5±0.3	268	1	MC12; Yang et al. (2014)
Andromeda VI	357.9429	24.5825	-11.5±0.2	111	0	MC12; Pritzl et al. (2002)
Cetus	6.5458	-11.0444	-11.3±0.2	630	0	MC12; Monelli et al. (2012)
ESO294-G010	6.6392	-41.8553	-11.2±0.3	232	1	MC12; Yang et al. (2014)
Andromeda I	11.4154	38.0375	-11.2±0.2	296	0	M16; Martínez-Vázquez et al. (2017)
Sculptor	15.0392	-33.7092	-10.8±0.1	536	1	M18; Martínez-Vázquez et al. (2016)
Aquarius	311.7158	-12.8481	-10.6±0.1	32	0	MC12; Ordoñez & Sarajedini (2016)
Phoenix	27.7763	-44.4447	-9.9±0.4	121	0	MC12; Ordoñez et al. (2014)
Leo II	168.3700	22.1517	-9.7±0.04	140	1	M18; Siegel & Majewski (2000)
Tucana	340.4567	-64.4194	-9.5±0.2	358	1	MC12; Bernard et al. (2009)
Andromeda III	8.8788	36.4989	-9.5±0.3	111	0	M16; Martínez-Vázquez et al. (2017)
Carina	100.4029	-50.9661	-9.43±0.05	83	1	M18; Coppola et al. (2015)
Leo P	155.4379	18.0881	-9.1±0.2	10	1	MC12; McQuinn et al. (2015)
Andromeda XXI	358.6996	42.4706	-9.1±0.3	41	0	M16; Cusano et al. (2015)
Ursa Minor	227.2854	67.2225	-9.03±0.05	82	1	M18; Nemec et al. (1988)
Andromeda XXV	7.5413	46.8614	-9.0±0.3	56	1	M16; Cusano et al. (2016)
Andromeda XIX	4.8938	35.0447	-9.0±0.6	31	0	MC12; Cusano et al. (2013)
Canes Venatici I	202.0146	33.5558	-8.80±0.06	23	0	MC12; Kuehn et al. (2008)
Sextans	153.2625	-1.6147	-8.72±0.06	227	1	M18; Vivas et al. (2019b)[c]
Draco	260.0517	57.9153	-8.71±0.05	267	1	M18; Kinemuchi et al. (2008)
Andromeda XXVIII	338.1729	31.2177	-8.7±0.4	85	0	S15; Martínez-Vázquez et al. (2017)
Crater II	177.3100	-18.4130	-8.2±0.1	99	1	T16a; Vivas et al. (2019a)[d]
Andromeda XV	18.5763	38.1197	-8.0±0.4	117	0	M16; Martínez-Vázquez et al. (2017)
Andromeda XXVII	9.3629	45.3869	-7.9±0.5	89	1	MC12; Cusano et al. (2017)
Leo T	143.7225	17.0514	-7.6±0.1	1	0	M18; Clementini et al. (2012)
Andromeda XVI	14.8763	32.3761	-7.3±0.3	8	0	M16; Monelli et al. (2016)
Andromeda XIII	12.9625	33.0044	-6.5±0.7	9	0	M16; Yang & Sarajedini (2012)
Andromeda XI	11.5821	33.8028	-6.3±0.6	15	0	M16; Yang & Sarajedini (2012)
Boötes I	210.0250	14.5000	-6.0±0.3	15	1	M18; Dall'Ora et al. (2006); Siegel (2006)
Hercules	247.7583	12.7917	-5.8±0.2	12	1	M18; Musella et al. (2012)[e]
Boötes III	209.3000	26.8000	-5.8±0.5	1	0	MC12; Sesar et al. (2014)
Sagittarius 2	298.1663	-22.8963	-5.7±0.1	5	1	L19; Joo et al. (2019)
Canes Venatici II	194.2917	34.3208	-5.2±0.3	2	1	M18; Greco et al. (2008)
Ursa Major I	158.7200	51.9200	-5.1±0.4	7	1	M18; Garofalo et al. (2013)
Leo IV	173.2375	-0.5333	-5.0±0.3	3	1	M18; Moretti et al. (2009)
Hydrus I	37.3890	-79.3089	-4.71±0.08	2	1	K18; Koposov et al. (2018)
Hydra II	185.4254	-31.9853	-4.6±0.4	1	1	M18; Vivas et al. (2016)
Carina II	114.1066	-57.9991	-4.5±0.1	3	1	T18; Torrealba et al. (2018)
Leo V	172.7900	2.2200	-4.4±0.4	3	1	M18; Medina et al. (2017)
Coma Berenices	186.7458	23.9042	-4.3±0.3	2	1	M18; Musella et al. (2009)
Aquarius II	338.4813	-9.3274	-4.3±0.1	1	0	T16b; Hernitschek et al. (2019)
Ursa Major II	132.8750	63.1300	-4.2±0.3	1	0	M18; Dall'Ora et al. (2012)
Grus II	331.0200	-46.4400	-3.9±0.2	1	1	DW15; This work
Grus I	344.1767	-50.1633	-3.5±0.6	2	1	M18; This work
Kim 2	317.2046	-51.1656	-3.3±0.6	0	1	M18; This work
Phoenix II	354.9975	-54.4061	-3.3±0.6	1	1	M18; This work
Boötes II	209.5000	12.8500	-2.9±0.7	1	0	M18; Sesar et al. (2014)

Table A1 – *continued* Number of RR Lyrae stars in dwarf galaxies

Galaxy	RA	Dec	M_V	N_{RRL}	$F_{2\times r_h}$ $^{(a)}$	References$^{(b)}$
Willman 1	162.3436	51.0501	-2.5±0.7	0	1	M18; Siegel et al. (2008)
Carina III	114.6298	-57.8997	-2.4±0.2	0	1	T18; Torrealba et al. (2018)
Segue 2	34.8167	20.1753	-1.9±0.9	1	1	M18; Boettcher et al. (2013)
Segue 1	151.7667	16.0819	-1.3±0.7	1	1	M18; Simon et al. (2011)

$^{(a)}$ $F_{2\times r_h}$=1 if the catalog of the RR Lyrae stars (or the search for them) goes beyond 2×r_h. If not, $F_{2\times r_h}$=0.
$^{(b)}$ References for the M_V values are given as acronyms: MC12:McConnachie (2012); DW15: Drlica-Wagner et al. (2015); S15: Slater et al. (2015); M16: Martin et al. (2016b); T16a; Torrealba et al. (2016a); T16b:Torrealba et al. (2016b); K18: Koposov et al. (2018); M18: Muñoz et al. (2018); T18: Torrealba et al. (2018); L19: Longeard et al. (2019).
$^{(c)}$ This is the most updated compilation. The RRL numbers here are also based on previous studies: Amigo (2012); Medina et al. (2018).
$^{(d)}$ This is the most updated compilation. The RRL numbers here are also based on previous studies: Joo et al. (2018); Monelli et al. (2018).
$^{(e)}$ We updated the number of RRL stars in Hercules including the outer RRL stars discovered by Garling et al. (2018).

de Estudos e Projetos, Fundação Carlos Chagas Filho de Amparo à Pesquisa do Estado do Rio de Janeiro, Conselho Nacional de Desenvolvimento Científico e Tecnológico and the Ministério da Ciência, Tecnologia e Inovação, the Deutsche Forschungsgemeinschaft and the Collaborating Institutions in the Dark Energy Survey.

The Collaborating Institutions are Argonne National Laboratory, the University of California at Santa Cruz, the University of Cambridge, Centro de Investigaciones Energéticas, Medioambientales y Tecnológicas-Madrid, the University of Chicago, University College London, the DES-Brazil Consortium, the University of Edinburgh, the Eidgenössische Technische Hochschule (ETH) Zürich, Fermi National Accelerator Laboratory, the University of Illinois at Urbana-Champaign, the Institut de Ciències de l'Espai (IEEC/CSIC), the Institut de Física d'Altes Energies, Lawrence Berkeley National Laboratory, the Ludwig-Maximilians Universität München and the associated Excellence Cluster Universe, the University of Michigan, the National Optical Astronomy Observatory, the University of Nottingham, The Ohio State University, the University of Pennsylvania, the University of Portsmouth, SLAC National Accelerator Laboratory, Stanford University, the University of Sussex, Texas A&M University, and the OzDES Membership Consortium.

The DES data management system is supported by the National Science Foundation under Grant Numbers AST-1138766 and AST-1536171. The DES participants from Spanish institutions are partially supported by MINECO under grants AYA2015-71825, ESP2015-66861, FPA2015-68048, SEV-2016-0588, SEV-2016-0597, and MDM-2015-0509, some of which include ERDF funds from the European Union. IFAE is partially funded by the CERCA program of the Generalitat de Catalunya. Research leading to these results has received funding from the European Research Council under the European Union's Seventh Framework Program (FP7/2007-2013) including ERC grant agreements 240672, 291329, and 306478. We acknowledge support from the Australian Research Council Centre of Excellence for All-sky Astrophysics (CAASTRO), through project number CE110001020, and the Brazilian Instituto Nacional de Ciência e Tecnologia (INCT) e-Universe (CNPq grant 465376/2014-2).

This manuscript has been authored by Fermi Research Alliance, LLC under Contract No. DE-AC02-07CH11359 with the U.S. Department of Energy, Office of Science, Office of High Energy Physics. The United States Government retains and the publisher, by accepting the article for publication, acknowledges that the United States Government retains a non-exclusive, paid-up, irrevocable, worldwide license to publish or reproduce the published form of this manuscript, or allow others to do so, for United States Government purposes.

TOPCAT (Taylor 2005), Aladin (Bonnarel et al. 2000; Boch & Fernique 2014), and Matplotlib (Hunter 2007) were used in this paper.

REFERENCES

Abbott T. M. C., et al., 2018, preprint, (arXiv:1801.03181)
Amigo P., 2012, PhD thesis, Pontificia Universidad Católica de Chile
Baker M., Willman B., 2015, AJ, 150, 160
Baldacci L., Rizzi L., Clementini G., Held E. V., 2005, A&A, 431, 1189
Bechtol K., et al., 2015, ApJ, 807, 50
Belokurov V., et al., 2007, ApJ, 658, 337
Benedict G. F., et al., 2011, AJ, 142, 187
Bernard E. J., et al., 2009, ApJ, 699, 1742
Bernard E. J., et al., 2010, ApJ, 712, 1259
Bernard E. J., et al., 2013, MNRAS, 432, 3047
Boch T., Fernique P., 2014, in Manset N., Forshay P., eds, Astronomical Society of the Pacific Conference Series Vol. 485, Astronomical Data Analysis Software and Systems XXIII. p. 277
Boettcher E., et al., 2013, AJ, 146, 94
Bonnarel F., et al., 2000, A&AS, 143, 33
Bose S., Deason A. J., Frenk C. S., 2018, ApJ, 863, 123
Bressan A., Marigo P., Girardi L., Salasnich B., Dal Cero C., Rubele S., Nanni A., 2012, MNRAS, 427, 127
Cáceres C., Catelan M., 2008, ApJS, 179, 242
Caputo F., 1997, MNRAS, 284, 994
Catelan M., 2009, Ap&SS, 320, 261
Catelan M., 2015, Pulsating Stars
Catelan M., Pritzl B. J., Smith H. A., 2004, ApJS, 154, 633
Clemens J. C., Crain J. A., Anderson R., 2004, in Moorwood A. F. M., Iye M., eds, Proc. SPIEVol. 5492, Ground-based Instrumentation for Astronomy. pp 331–340, doi:10.1117/12.550069
Clementini G., Cignoni M., Contreras Ramos R., Federici L., Ripepi V., Marconi M., Tosi M., Musella I., 2012, ApJ, 756, 108
Clementini G., et al., 2019, A&A, 622, A60
Conn B. C., Jerjen H., Kim D., Schirmer M., 2018a, ApJ, 852, 68
Conn B. C., Jerjen H., Kim D., Schirmer M., 2018b, ApJ, 857, 70
Contenta F., Gieles M., Balbinot E., Collins M. L. M., 2017, MNRAS, 466, 1741
Coppola G., et al., 2015, ApJ, 814, 71
Cusano F., et al., 2013, ApJ, 779, 7
Cusano F., et al., 2015, ApJ, 806, 200
Cusano F., et al., 2016, preprint, (arXiv:1606.06862)
Cusano F., et al., 2017, ApJ, 851, 9
Dall'Ora M., et al., 2006, The Astrophysical Journal, 653, L109
Dall'Ora M., et al., 2012, ApJ, 752, 42

Deason A. J., Wetzel A. R., Garrison-Kimmel S., Belokurov V., 2015, MNRAS, 453, 3568
Drlica-Wagner A., et al., 2015, ApJ, 813, 109
Drlica-Wagner A., et al., 2016, ApJ, 833, L5
Erkal D., et al., 2018, MNRAS, 481, 3148
Fardal M. A., van der Marel R. P., Sohn S. T., del Pino Molina A., 2019, MNRAS, p. 797
Fellhauer M., et al., 2007, MNRAS, 375, 1171
Fernley J., Skillen I., Carney B. W., Cacciari C., Janes K., 1998, Monthly Notices of the Royal Astronomical Society, 293, L61
Fiorentino G., et al., 2015, ApJ, 798, L12
Fiorentino G., et al., 2017, A&A, 599, A125
Flaugher B., et al., 2015, AJ, 150, 150
Fritz T. K., Carrera R., Battaglia G., Taibi S., 2018, arXiv e-prints,
Garling C., et al., 2018, ApJ, 852, 44
Garofalo A., et al., 2013, ApJ, 767, 62
Greco C., et al., 2008, ApJ, 675, L73
Grillmair C. J., 2006, ApJ, 645, L37
Hernitschek N., et al., 2019, ApJ, 871, 49
Holl B., et al., 2018, A&A, 618, A30
Horne J. H., Baliunas S. L., 1986, ApJ, 302, 757
Hunter J. D., 2007, Computing in Science & Engineering, 9, 90
Jerjen H., Conn B., Kim D., Schirmer M., 2018, preprint, (arXiv:1809.02259)
Jethwa P., Erkal D., Belokurov V., 2016, MNRAS, 461, 2212
Ji A. P., Simon J. D., Frebel A., Venn K. A., Hansen T. T., 2019, ApJ, 870, 83
Joo S.-J., et al., 2018, ApJ, 861, 23
Joo S.-J., et al., 2019, arXiv e-prints, p. arXiv:1904.01599
Kallivayalil N., et al., 2018, ApJ, 867, 19
Kim D., Jerjen H., 2015, ApJ, 808, L39
Kim D., Jerjen H., Milone A. P., Mackey D., Da Costa G. S., 2015, ApJ, 803, 63
Kinemuchi K., Harris H. C., Smith H. A., Silbermann N. A., Snyder L. A., La Cluyzé A. P., Clark C. L., 2008, AJ, 136, 1921
Koposov S. E., Belokurov V., Torrealba G., Evans N. W., 2015, ApJ, 805, 130
Koposov S. E., et al., 2018, MNRAS, 479, 5343
Koposov S. E., et al., 2019, MNRAS, 485, 4726
Kuehn C., et al., 2008, ApJ, 674, L81
Lang D., Hogg D. W., Mierle K., Blanton M., Roweis S., 2010, AJ, 137, 1782
Layden A. C., Ritter L. A., Welch D. L., Webb T. M. A., 1999, AJ, 117, 1313
Li T. S., et al., 2018, ApJ, 857, 145
Lindegren L., et al., 2018, A&A, 616, A2
Longeard N., et al., 2019, arXiv e-prints, p. arXiv:1902.02780
Luque E., et al., 2016, MNRAS, 458, 603
Luque E., et al., 2017, MNRAS, 468, 97
Marconi M., et al., 2015, ApJ, 808, 50
Martin N. F., et al., 2015, ApJ, 804, L5
Martin N. F., et al., 2016a, ApJ, 830, L10
Martin N. F., et al., 2016b, ApJ, 833, 167
Martínez-Vázquez C. E., et al., 2016, MNRAS, 462, 4349
Martínez-Vázquez C. E., et al., 2017, ApJ, 850, 137
Mau S., et al., 2019, ApJ, 875, 154
McConnachie A. W., 2012, AJ, 144, 4
McQuinn K. B. W., et al., 2015, ApJ, 812, 158
Medina G. E., et al., 2017, ApJ, 845, L10
Medina G. E., et al., 2018, ApJ, 855, 43
Monelli M., et al., 2010, ApJ, 720, 1225
Monelli M., et al., 2012, MNRAS, 422, 89
Monelli M., et al., 2016, ApJ, 819, 147
Monelli M., Fiorentino G., Bernard E. J., Martínez-Vázquez C. E., Bono G., Gallart C., Dall'Ora M., Stetson P. B., 2017, ApJ, 842, 60
Monelli M., et al., 2018, MNRAS, 479, 4279
Moretti M. I., et al., 2009, ApJ, 699, L125
Morganson E., et al., 2018, PASP, 130, 074501
Muñoz R. R., Côté P., Santana F. A., Geha M., Simon J. D., Oyarzún G. A., Stetson P. B., Djorgovski S. G., 2018, ApJ, 860, 66
Muraveva T., Delgado H. E., Clementini G., Sarro L. M., Garofalo A., 2018, Monthly Notices of the Royal Astronomical Society, 481, 1195
Musella I., et al., 2009, ApJ, 695, L83
Musella I., et al., 2012, ApJ, 756, 121
Mutlu-Pakdil B., et al., 2018, ApJ, 863, 25
Nemec J. M., Wehlau A., Mendes de Oliveira C., 1988, AJ, 96, 528
Ordoñez A. J., Sarajedini A., 2016, MNRAS, 455, 2163
Ordoñez A. J., Yang S.-C., Sarajedini A., 2014, ApJ, 786, 147
Pace A. B., Li T. S., 2019, ApJ, 875, 77
Pardy S. A., et al., 2019, arXiv e-prints, p. arXiv:1904.01028
Pietrzyński G., et al., 2019, Nature, 567, 200
Pritzl B. J., Armandroff T. E., Jacoby G. H., Da Costa G. S., 2002, AJ, 124, 1464
Saha A., et al., 2010, AJ, 140, 1719
Saha A., et al., 2019, ApJ, 874, 30
Salaris M., Chieffi A., Straniero O., 1993, ApJ, 414, 580
Sales L. V., et al., 2008, MNRAS, 389, 1391
Sales L. V., Navarro J. F., Cooper A. P., White S. D. M., Frenk C. S., Helmi A., 2011, MNRAS, 418, 648
Sales L. V., Navarro J. F., Kallivayalil N., Frenk C. S., 2017, MNRAS, 465, 1879
Sandage A., 1990, ApJ, 350, 603
Sanderson R. E., Secunda A., Johnston K. V., Bochanski J. J., 2017, MNRAS, 470, 5014
Schechter P. L., Mateo M., Saha A., 1993, PASP, 105, 1342
Schlafly E. F., Finkbeiner D. P., 2011, ApJ, 737, 103
Schlegel D. J., Finkbeiner D. P., Davis M., 1998, ApJ, 500, 525
Sesar B., et al., 2013, ApJ, 776, 26
Sesar B., et al., 2014, ApJ, 793, 135
Shipp N., et al., 2018, ApJ, 862, 114
Siegel M. H., 2006, ApJ, 649, L83
Siegel M. H., Majewski S. R., 2000, AJ, 120, 284
Siegel M. H., Shetrone M. D., Irwin M., 2008, AJ, 135, 2084
Simon J. D., 2019, arXiv e-prints, p. arXiv:1901.05465
Simon J. D., et al., 2011, ApJ, 733, 46
Slater C. T., Bell E. F., Martin N. F., Tollerud E. J., Ho N., 2015, ApJ, 806, 230
Soszyński I., et al., 2014, Acta Astron., 64, 177
Soszyński I., et al., 2016, Acta Astron., 66, 131
Stetson P. B., 1987, PASP, 99, 191
Stetson P. B., 1994, PASP, 106, 250
Stetson P. B., Fiorentino G., Bono G., Bernard E. J., Monelli M., Iannicola G., Gallart C., Ferraro I., 2014, PASP, 126, 616
Stringer K. M., et al., 2019, arXiv e-prints, p. arXiv:1905.00428
Suntzeff N. B., Kinman T. D., Kraft R. P., 1991, ApJ, 367, 528
Taylor M. B., 2005, in Shopbell P., Britton M., Ebert R., eds, Astronomical Society of the Pacific Conference Series Vol. 347, Astronomical Data Analysis Software and Systems XIV. p. 29
The Dark Energy Survey Collaboration 2005, arXiv e-prints, pp astro–ph/0510346
Tody D., 1986, in Crawford D. L., ed., Proc. SPIEVol. 627, Instrumentation in astronomy VI. p. 733, doi:10.1117/12.968154
Tody D., 1993, in Hanisch R. J., Brissenden R. J. V., Barnes J., eds, Astronomical Society of the Pacific Conference Series Vol. 52, Astronomical Data Analysis Software and Systems II. p. 173
Torrealba G., Koposov S. E., Belokurov V., Irwin M., 2016a, MNRAS, 459, 2370
Torrealba G., et al., 2016b, MNRAS, 463, 712
Torrealba G., et al., 2018, MNRAS, 475, 5085
Valdes F., Gruendl R., DES Project 2014, in Manset N., Forshay P., eds, Astronomical Society of the Pacific Conference Series Vol. 485, Astronomical Data Analysis Software and Systems XXIII. p. 379
Vivas A. K., Zinn R., 2006, AJ, 132, 714
Vivas A. K., et al., 2016, AJ, 151, 118
Vivas A. K., et al., 2017, AJ, 154, 85

Vivas A. K., Walker A. R., Martínez-Vázquez C. E., et al. 2019a, MNRAS, p. submitted
Vivas A. K., Alonso-García J., Mateo M., Walker A., Howard B., 2019b, AJ, 157, 35
Walker A. R., 1989, PASP, 101, 570
Walker A. R., 2012, Ap&SS, 341, 43
Walker M. G., et al., 2016, ApJ, 819, 53
Wheeler C., Oñorbe J., Bullock J. S., Boylan-Kolchin M., Elbert O. D., Garrison-Kimmel S., Hopkins P. F., Kereš D., 2015, MNRAS, 453, 1305
White S. D. M., Frenk C. S., 1991, ApJ, 379, 52
Willman B., et al., 2005a, AJ, 129, 2692
Willman B., et al., 2005b, ApJ, 626, L85
Yang S.-C., Sarajedini A., 2012, MNRAS, 419, 1362
Yang S.-C., Wagner-Kaiser R., Sarajedini A., Kim S. C., Kyeong J., 2014, ApJ, 784, 76
York D. G., et al., 2000, AJ, 120, 1579
Zinn R., Horowitz B., Vivas A. K., Baltay C., Ellman N., Hadjiyska E., Rabinowitz D., Miller L., 2014, ApJ, 781, 22

AFFILIATIONS

[1] *Cerro Tololo Inter-American Observatory, National Optical Astronomy Observatory, Casilla 603, La Serena, Chile*
[2] *Department of Physics & Astronomy, University of Rochester, 500 Joseph C. Wilson Blvd, Rochester, NY 14627, USA*
[3] *George P. and Cynthia Woods Mitchell Institute for Fundamental Physics and Astronomy, and Department of Physics and Astronomy, Texas A&M University, College Station, TX 77843, USA*
[4] *Instituto de Física, UFRGS, Caixa Postal 15051, Porto Alegre, RS - 91501-970, Brazil*
[5] *Laboratório Interinstitucional de e-Astronomia - LIneA, Rua Gal. José Cristino 77, Rio de Janeiro, RJ - 20921-400, Brazil*
[6] *University of Pennsylvania Department of Physics & Astronomy, 209 South 33rd Street, Philadelphia, PA 19104-6396*
[7] *Fermi National Accelerator Laboratory, P. O. Box 500, Batavia, IL 60510, USA*
[8] *Kavli Institute for Cosmological Physics, University of Chicago, Chicago, IL 60637, USA*
[9] *LSST, 933 North Cherry Avenue, Tucson, AZ 85721, USA*
[10] *Physics Department, 2320 Chamberlin Hall, University of Wisconsin-Madison, 1150 University Avenue Madison, WI 53706-1390*
[11] *Lawrence Berkeley National Laboratory, 1 Cyclotron Road, Berkeley, CA 94720, USA*
[12] *Observatories of the Carnegie Institution for Science, 813 Santa Barbara St., Pasadena, CA 91101, USA*
[13] *Kavli Institute for Particle Astrophysics & Cosmology, P. O. Box 2450, Stanford University, Stanford, CA 94305, USA*
[14] *Instituto de Fisica Teorica UAM/CSIC, Universidad Autonoma de Madrid, 28049 Madrid, Spain*
[15] *CNRS, UMR 7095, Institut d'Astrophysique de Paris, F-75014, Paris, France*
[16] *Sorbonne Universités, UPMC Univ Paris 06, UMR 7095, Institut d'Astrophysique de Paris, F-75014, Paris, France*
[17] *Department of Physics & Astronomy, University College London, Gower Street, London, WC1E 6BT, UK*
[18] *SLAC National Accelerator Laboratory, Menlo Park, CA 94025, USA*
[19] *Centro de Investigaciones Energéticas, Medioambientales y Tecnológicas (CIEMAT), Madrid, Spain*
[20] *Department of Astronomy, University of Illinois at Urbana-Champaign, 1002 W. Green Street, Urbana, IL 61801, USA*
[21] *National Center for Supercomputing Applications, 1205 West Clark St., Urbana, IL 61801, USA*
[22] *Observatório Nacional, Rua Gal. José Cristino 77, Rio de Janeiro, RJ - 20921-400, Brazil*
[23] *Department of Physics, IIT Hyderabad, Kandi, Telangana 502285, India*
[24] *Santa Cruz Institute for Particle Physics, Santa Cruz, CA 95064, USA*
[25] *Institut d'Estudis Espacials de Catalunya (IEEC), 08034 Barcelona, Spain*
[26] *Institute of Space Sciences (ICE, CSIC), Campus UAB, Carrer de Can Magrans, s/n, 08193 Barcelona, Spain*
[27] *Department of Physics, Stanford University, 382 Via Pueblo Mall, Stanford, CA 94305, USA*
[28] *Center for Cosmology and Astro-Particle Physics, The Ohio State University, Columbus, OH 43210, USA*
[29] *Department of Physics, The Ohio State University, Columbus, OH 43210, USA*
[30] *Center for Astrophysics | Harvard & Smithsonian, 60 Garden Street, Cambridge, MA 02138, USA*
[31] *Australian Astronomical Optics, Macquarie University, North Ryde, NSW 2113, Australia*
[32] *Lowell Observatory, 1400 Mars Hill Rd, Flagstaff, AZ 86001, USA*
[33] *Department of Astronomy, University of Michigan, Ann Arbor, MI 48109, USA*
[34] *Department of Physics, University of Michigan, Ann Arbor, MI 48109, USA*
[35] *Institució Catalana de Recerca i Estudis Avançats, E-08010 Barcelona, Spain*
[36] *Institut de Física d'Altes Energies (IFAE), The Barcelona Institute of Science and Technology, Campus UAB, 08193 Bellaterra (Barcelona) Spain*
[37] *Department of Astrophysical Sciences, Princeton University, Peyton Hall, Princeton, NJ 08544, USA*
[38] *School of Physics and Astronomy, University of Southampton, Southampton, SO17 1BJ, UK*
[39] *Brandeis University, Physics Department, 415 South Street, Waltham MA 02453*
[40] *Instituto de Física Gleb Wataghin, Universidade Estadual de Campinas, 13083-859, Campinas, SP, Brazil*
[41] *Argonne National Laboratory, 9700 South Cass Avenue, Lemont, IL 60439, USA*

This paper has been typeset from a TEX/LATEX file prepared by the author.